Behaviour of cold-formed concrete-filled dual steel stiffened tubular short columns

Zhang, Jun-Hua; Shao, Yong-Bo; Hassanein, Mostafa Fahmi; Cashell, Katherine A.; Hadzima-Nyarko, Marijana

Permanent link / Trajna poveznica: https://urn.nsk.hr/urn:nbn:hr:133:677851

Download date / Datum preuzimanja: **2025-02-22**

GRAĐEVINSKI I ARHITEKTONSKI FAKULTET OSIJEK
Faculty of Civil Engineering and Architecture Osijek

Repository / Repozitorij:

Repository GrAFOS - Repository of Faculty of Civil Engineering and Architecture Osijek

SVEUČILIŠTE JOSIPA JURJA STROSSMAYERA U OSIJEKU

dabar
DIGITALNI AKADEMSKI ARHIVI I REPOZITORIJI

Behaviour of cold-formed concrete-filled dual steel stiffened tubular short columns

Jun-Hua Zhang [a], Yong-Bo Shao [a,*], M.F. Hassanein [a,b,*], K.A. Cashell [c], Marijana Hadzima-Nyarko [d]

[a] School of Civil Engineering and Geomatics, Southwest Petroleum University, Chengdu, Sichuan 610500, PR China
[b] Department of Structural Engineering, Faculty of Engineering, Tanta University, Tanta, Egypt
[c] Department of Civil Environmental and Geomatic Engineering, UCL, London, UK
[d] Faculty of Civil Engineering and Architecture, Josip Juraj Strossmayer University of Osijek, Vladimira Preloga 3, 31000 Osijek, Croatia

ARTICLE INFO

ABSTRACT

This paper presents an experimental and numerical investigation into the behaviour of cold-formed concrete-filled dual steel-stiffened tubular (CFDSST) short columns under axial compressive load. This new composite column is fabricated from four cold-formed lipped angles to make the outer steel tube and a concentrically-placed steel tube located inside with concrete filled inside both the inner and outer tubes. The lips in the outer steel section behave as longitudinal stiffeners. To investigate the axial compression behaviour of these columns, fourteen CFDSSTs were designed and fabricated as well as two concrete-filled stiffened steel tubular (CFSST) columns and two concrete-filled double steel stiffened tubular (D-CFSST) columns for comparison. The columns failed due to local buckling of the outer steel tubes. The columns were modelled using finite element analysis and the accuracy and reliability of the numerical data was determined by comparing the numerical and experimental results. The validated model was employed to conduct a parametric analysis to investigate the behaviour of CFDSST columns with different variables and properties. The results show that the ultimate strength of CFDSST columns is most significantly influenced by the presence and strength of the sandwiched concrete between the two steel sections. The paper also presents an analysis of the accuracy and reliability of different international codified methods for predicting the load-carrying capacity of CFDSSTs.

1. Introduction

Concrete-filled steel tubular (CFST) columns, as shown in Fig. 1(a), are an important structural solution in applications that require high load-carrying capacity. CFST columns combine the favourable properties of the constituent materials, steel and concrete, to be able to withstand extreme loads. Previous research has shown that CFST columns exhibit excellent seismic and compressive resistance behaviour [1–6]. Owing to the presence of the outer steel tube, CFST columns tend to have higher bending stiffness compared with similarly-sized traditional reinforced concrete columns [7]. The confining effect on the concrete provided by the outer steel tube adds to their capacity, and the presence of the concrete core can also prevent or delay local buckling of the steel tube. Additionally, the construction cost and time can be reduced because the steel tube acts as external formwork in the concrete pouring process. For these reasons, CFST columns have become increasingly popular in challenging engineering applications in recent years.

Whilst the advantages of CFST columns are clear, there are some challenges also associated with their use and behaviour. Firstly, in extremely high-loading scenarios such as in large-span structures and high-rise buildings, very large cross-sections may be required. For example, the diameter of the CFST column in the first storey of ShenZhen Saibo Plaza Building in China is 1600 mm which significantly reduces the useful interior space [8,9]. In addition, the benefits to the cross-sectional strength through confinement of the concrete are less significant in relatively large sections [10,11]. Secondly, the confinement effect is not effective in the elastic stage of CFST columns because the Poisson's ratio of steel is greater than that of concrete. This phenomenon reduces until the development of initial cracks in the concrete and lateral expansion of the concrete becomes larger than that of steel tubes. This phenomenon can be more pronounced for CFSTs with high strength concrete and thin-walled steel tubes [12]. Finally, the fire

---

resistance and the load-carrying capacity of CFST columns after the peak load has been reached cannot be guaranteed in some special cases. As a results of these disadvantages, some innovations have been proposed in the formation of composite columns [8,9,13–20], such as the use of high strength concrete (HSC) or ultra-high strength concrete (UHSC), stiffeners to the steel tubes and the addition of internal steel tubes.

To date, there has been a considerable amount of experimental and numerical research studies into the behaviour of concrete-filled dual steel tubular columns. These are referred to as CFDST herein, as given in other publications, and a typical cross-section is presented in Fig. 1(b); it is noteworthy that CFDSTs may or may not have concrete included in the inner core region, and it is included herein as this is most relevant to the work presented. These are made using two metallic tubes with different dimensions concentrically positioned one inside the other, and concrete filling the entire cross-section. These sections tend to be smaller than CFSTs to carry comparable loads due to the addition of the inner steel tubes, resulting in efficient use of floor space and a lighter overall structure. Additionally, the integrity of these type of composite columns in some special cases is more reliable than CFSTs because the inner tube is protected by the infill concrete. The key properties of CFDST columns include high strength as well as excellent ductility and stiffness [19–27]. Ekmekyapar and Al-Eliwi [20] conducted tests on the repair and strengthening behaviour of stressed and deformed CFST columns by converting them into CFDST columns. The test results showed that CFDST columns can be effectively used to repair CFST columns to increase their compression resistance, ductility and stiffness. Therefore, CFDST columns can be used as a strengthening solution in critical areas of the buildings.

Previous research has shown that including stiffeners in the cross-section can effectively delay local buckling of the outer steel tubes [28–30]. In addition, lateral expansion of the steel tube can be reduced by using embedded stiffeners as shown in Fig. 2. In this case, the stiffeners enhance the bond between the steel tube and the concrete in the inelastic stage thus reducing the development of disproportionate deformations in the steel tube and concrete due to incompatibilities of the Poisson's ratio of steel and concrete. Moreover, using stiffeners can enhance the resistance of the section against lateral loads [31]. However, the research into concrete-filled dual stiffened steel tubular (CFDSST) columns is limited. A schematic of a CFDSST section is shown in Fig. 1(c). Wang et al. [32] carried out a series of experiments to investigate the behaviour of CFDSST columns with a square stiffened hollow (SHS) outer section and a circular hollow inner section (CHS) under axial loading. The test results showed that the strength and ductility of the columns were excellent and enhanced by the presence of the inner steel tube and the stiffeners. The columns failed by local outward buckling of the outer square steel tube only when the sandwiched
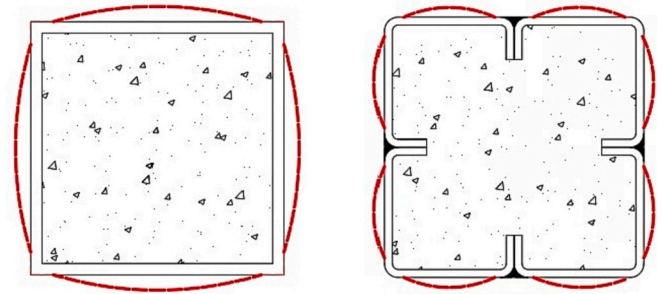

Fig. 2. Buckling modes of steel and composite sections.

concrete was crushed and the stiffeners buckled. Additionally, Wang et al. [33–35] studied the behaviour of CFDSST columns under eccentric compression and the flexural and seismic performance of CFDSST columns. Zhang et al. [36] analysed the behaviour of CFDSST columns with inner circular tubes filled with UHSC through FE analysis.

It is clear that despite the promising performance of CFDSST members that there is a lack of experimental or numerical performance data in the literature, and therefore their behaviour is not fully understood. Therefore, the current paper presents an experimental and numerical study into the axial behaviour of CFDSST columns with inner square tubes. A total of 18 tests were conducted comprising 14 CFDSSTs, as shown in Fig. 3(a), and four other specimens made up of two CFSSTs (Fig. 3(b)) and two concrete-filled double-skin steel tubular columns without core concrete (abbreviated as D-CFSST in this paper, as shown in Fig. 3(c)) for comparison. The paper proceeds with a description of the tests and the results are presented and discussed. A finite element (FE) model was developed and is then described. The accuracy and reliability of the model were validated by comparison with the test results. Thereafter, the details of a parametric analysis are presented to study the behaviour of CFDSST columns with different variables. In the final portion of the paper, the design resistances calculated by using international specifications such as Eurocode 4 [37], BS5400 [38] and DBJ1315–2010 [39] are compared with the experimentally obtained resistances and design recommendations are provided.

2. Experimental programme

2.1. General

A total of eighteen specimens were designed and fabricated for the experimental programme, including fourteen CFDSST columns, two CFSST columns and two D-CFSST columns. The cross-sections of the
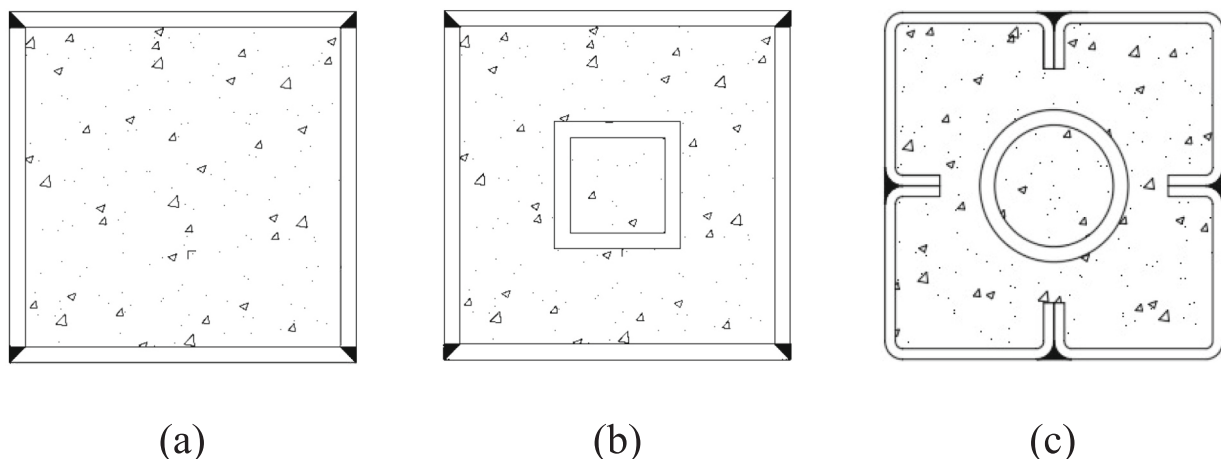

(a)   (b)   (c)

Fig. 1. Typical cross-sections of composite columns including (a) CFST (b) CFDST and (c) CFDSST.
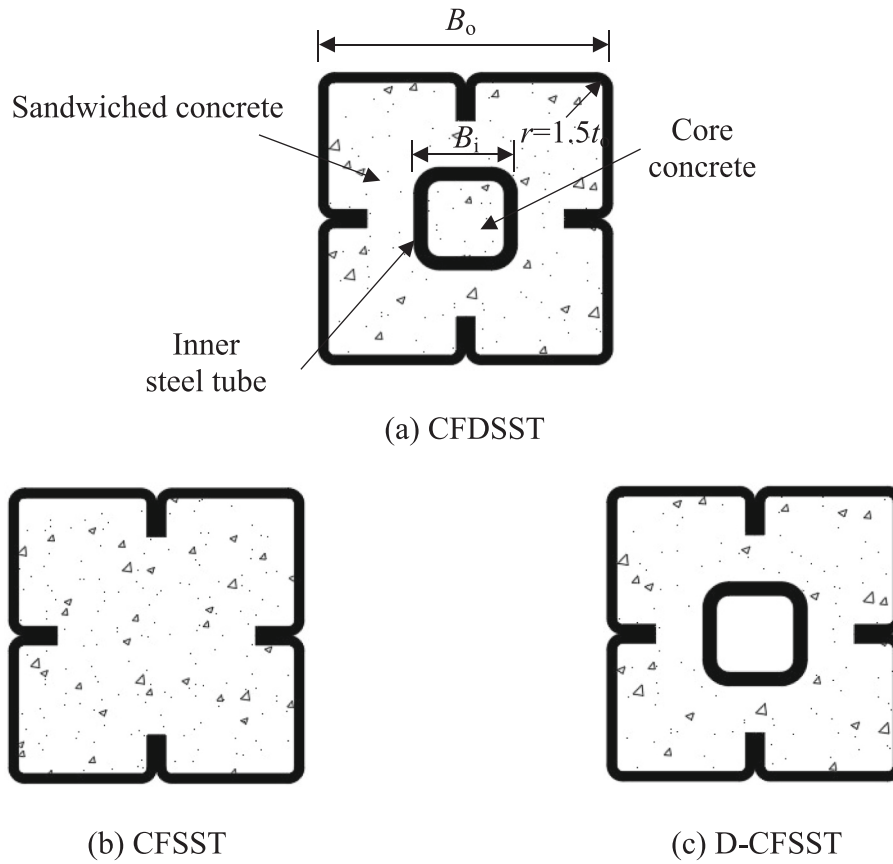
(a) CFDSST

(b) CFSST

(c) D-CFSST

Fig. 3. Cross-sections of the test specimens.

specimens are shown in Fig. 3. The geometrical and material properties of the specimens are presented in Table 1. The ultimate axial bearing capacities of the experiments ($N_{ul,Exp}$) are also included in Table 1, where B_o is the overall width of steel tube, t_o and t_i are the thicknesses of the outer and inner steel tubes, respectively, f_{yo} and f_{yi} are the yield strengths of the outer and inner steel tubes, f_{cu} is the concrete compressive strength. The height of the longitudinal stiffeners h_s was 25 mm for all tests. The first term in the specimen designations is either "S" or "SS" which refer to the 4 CFSSTs (G1) and D-CFSSTs (G2) included for

comparison and the CFDSST columns (G3-G6), respectively. The next terms is either 160 or 180 and represents the width of the outer steel tubes (B_o), in mm. The last number (between 1 and 7) refers to an individual specimen, with individual characteristics (like geometry and material properties). The symbol "#" is used for the D-CFSST columns.

The main experimental parameters examined in this programme were (i) the presence, or not, of an inner steel tube; (ii) the inclusion of core concrete; (iii) the concrete compressive strength; and (iv) the D/B_o ratio of the cross-section. The height (L) of the specimens was three

Table 1
Parameters and test results of CFDSST columns under axial loading.

Groups	Specimens	B_o (mm)	t_o (mm)	f_{yo} (MPa)	f_{cu} (MPa)	B_i (mm)	t_i (mm)	f_{yi} (MPa)	L (mm)	DI	SI	$N_{ul.Exp}$ (kN)	$N_{ul.FE}$ (kN)	$\frac{N_{ul.FE}}{N_{ul.Exp}}$
G1	S-160	160	2.0	281	49.18	–	–	–	480	1.71	1.136	1617	1502	0.93
	S-180	180	2.0	281	49.18	–	–	–	540	1.55	1.030	1765	1836	1.04
G2	S-160#	160	2.0	281	49.18	80	4	425	480	2.92	0.952	1595	1720	1.08
	S-180#	180	2.0	281	49.18	80	4	425	540	1.95	1.050	2064	2049	0.99
G3	SS-160-1	160	2.0	281	49.18	80	4	425	480	1.94	1.106	2090	1970	0.94
	SS-160-2	160	2.0	281	53.58	80	4	425	480	2.00	1.042	2066	2070	1.00
	SS-160-3	160	2.0	281	70.30	80	4	425	480	1.40	1.182	2770	2435	0.88
G4	SS-160-4	160	2.0	281	49.18	80	4.2	533	480	2.96	1.047	2147	2111	0.98
	SS-160-5	160	2.7	329	49.18	80	4.2	533	480	3.10	0.968	2237	2313	1.03
	SS-160-6	160	2.0	281	49.18	60	4.2	533	480	3.54	0.996	1878	1940	1.03
	SS-160-7	160	2.7	329	49.18	60	4.2	533	480	4.03	0.943	2025	2184	1.08
G5	SS-180-1	180	2.0	281	49.18	80	4	425	540	2.02	1.096	2389	2302	0.96
	SS-180-2	180	2.0	281	53.58	80	4	425	540	2.01	1.061	2441	2408	0.99
	SS-180-3	180	2.0	281	70.30	80	4	425	540	1.29	1.145	3167	2890	0.91
G6	SS-180-4	180	2.0	281	49.18	80	4.2	533	540	3.62	0.998	2336	2451	1.05
	SS-180-5	180	2.7	329	49.18	80	4.2	533	540	2.64	0.925	2447	2718	1.11
	SS-180-6	180	2.0	281	49.18	60	4.2	533	540	4.92	0.974	2118	2278	1.08
	SS-180-7	180	2.7	329	49.18	60	4.2	533	540	2.01	0.970	2404	2534	1.05
											Mean			1.008
											COV			0.064

times the width of the outer steel tube (B_o). In addition, the second moment of area of the longitudinal stiffeners (I_s) was defined to meet the requirement proposed by Tao et al. [40] and given in Eq. (1):

$$I_s = 3.1 \times 10^{-4} \left(\frac{0.5B_o - 2t_o}{t_o} \right)^{3.5} \frac{f_{yo}}{280} t_o^4 \tag{1}$$

2.2. Material properties

Based on the availability of materials in the market at the time of specimen preparation, carbon steel grade Q235 was used for the outer steel tubes and Q355 was used for the inner steel tubes and endplates in this experimental investigation. The properties of the carbon steel used for tube specimens were determined by conducting a series of tensile coupon tests. The coupon dimensions conformed to the Australian Standard AS 1391 [41] for the tensile testing of metals using 12.5 mm wide coupons with a gauge length of 50 mm, as detailed in Fig. 4. The actual yield strength of carbon steels can be seen as Table 1, which is taken as the average value of at least three repeat tensile tests. Note that since the width of the inner tubes was around 60–80 mm, the compactness of the concrete inside the inner tube is very important [42]. Therefore, during the specimen preparation, the concrete was compacted carefully using a vibrator to increase the interlocking between the steel and concrete components.

Three concrete mixes with target cube compressive strengths of 40 MPa, 50 MPa and 70 MPa were employed in the test programme. The sandwiched concrete and the core concrete were filled with the same concrete mix, and the mix designs are presented in Table 2, together with the concrete cube strengths (f_{cu}). In the table, the *w/c* ratio refers to the water to cement ratio. It is also noteworthy that the mix design for C70 contained fly ash and silica fume, which are cement replacement products. They replaced 22% (fly ash) and 8% (silica fume) of the cement, with cement making up the remaining 70% in the mix design.

The CFDSST columns comprised two endplates, four lipped angles to create the outer steel tube, an inner steel section, sandwiched concrete between the two steel tubes and core concrete inside the inner steel section. The manufacturing process of the lipped angles to create the outer steel section is shown in Fig. 5. The specimens were made by first welding the inner steel tubes to the bottom endplate, which had a thickness of 20 mm. The four lipped angles were then welded together and welded to the bottom endplate. The concrete was filled into the steel tubes in the laboratory of the Southwest Petroleum University, China, and compacted by a vibrator. After 14 days of curing, a layer of high-strength mortar was applied to the top of each specimen to ensure uniformity of the top surface. 28 days after pouring the concrete, another endplate with a thickness of 20 mm was welded to the upper end of each column. This process and the final specimens are shown in Fig. 6. It is noteworthy that the extended flanges which are in contact between adjacent angles (*i.e.* the longitudinal stiffeners) were welded together by spot welding for positioning purposes only and their contact was maintained mainly by the pressure of the infilled concrete on their inner surfaces.

Table 2
Concrete mix designs.

Concrete mix	Unit	C40	C50	C70
Cement	kg/m^3	400	480	387
Coarse aggregate	kg/m^3	1080	1070	1015
Fine aggregate	kg/m^3	720	720	677
Water	kg/m^3	180	175	155
w/c	%	0.45	0.36	0.28
Fly ash	kg/m^3	–	–	122.10
Silica fume	kg/m^3	–	–	44.40
Water reducer	kg/m^3	0.40	0.48	1.38
Concrete cube strength (f_{cu})	MPa	49.18	53.58	70.30

2.3. Test methodology

The columns were tested in the structures laboratory at the Southwest University of Science and Technology, China using a 10,000 kN capacity hydraulic testing machine. The columns were instrumented with a series of strain gauges and dial (displacement) gauges at locations as shown in Fig. 7 and Fig. 8, respectively. There were two strain gauges on each side (labelled A-D) of the columns, with one in the longitudinal (L) and another in the transverse (T) direction. Fig. 8 shows a schematic view of the test set-up. The strains at the contact between the steel section inner surface and the concrete infill were not measured during the experiments, as they have been shown previously to be identical [43]. All columns were positioned in the testing machine to ensure perfect alignment and verticality. Previous research [44] found that premature local crushing phenomena was observed at the end of short columns and researchers suggested using clamping devices on at ends of the columns to prevent localized crushing in this region. Accordingly, similar clamping devices were used in this programme as shown in Fig. 8. Additionally, the ultimate axial resistances ($N_{ul,Exp}$) of the test specimens were predicted numerically, using the finite element model described in this paper, before testing. Before the axial load reached a value equal to $0.5N_{ul,Exp}$, load control was adopted with a load interval of $0.25N_{ul,Exp}$ and a loading rate of 5 N/s initially, and at each level the load was held for about 2 min. After that, displacement control was employed with a displacement rate of 0.5 mm/min until the axial force in the column in the descending branch of the response reached approximately 60% of the ultimate load capacity. This testing protocol was adopted following observations from other research programmes. Tao et al. [45–46] showed that the response in the ascending branch of the load-displacement curve can be controlled appropriately by load-control, while this is more challenging during the softening phase, post- peak load. It was found that to achieve the most accurate response in the softening phase, displacement-control should be employed with a slow rate of displacement applied. Accordingly, in the current tests, load control was employed up to 50% of the peak load and then the controller was switched to displacement control to measure the ultimate load and the post-peak behaviour. This approach was also adopted by many other researchers (*e.g.* [47–49]).
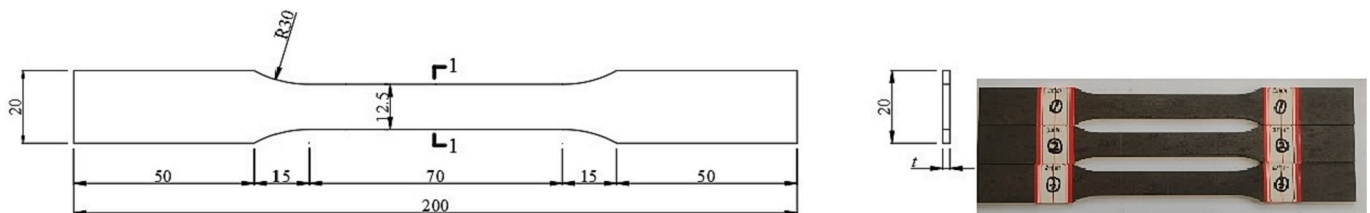

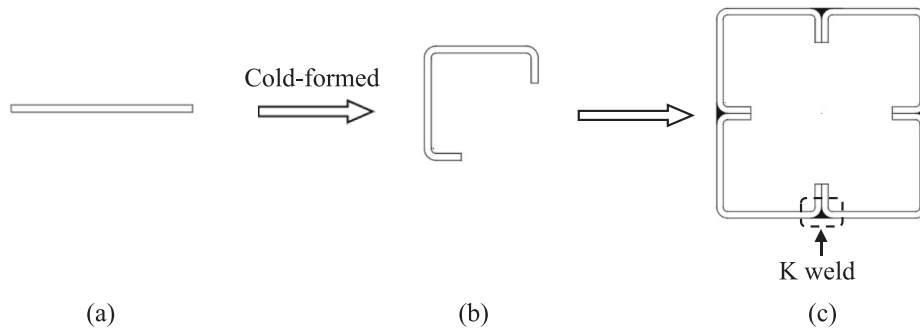**Fig. 4.** Dimensions of test coupon.

Fig. 5. Process of making the outer steel tube from steel plate to final tubular section.
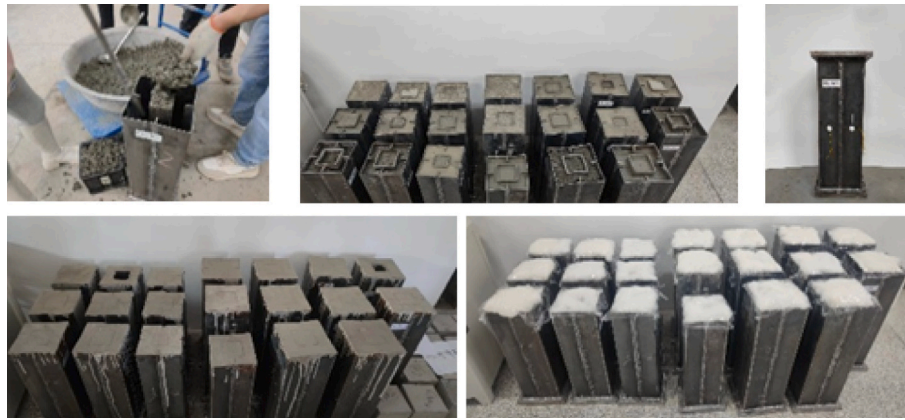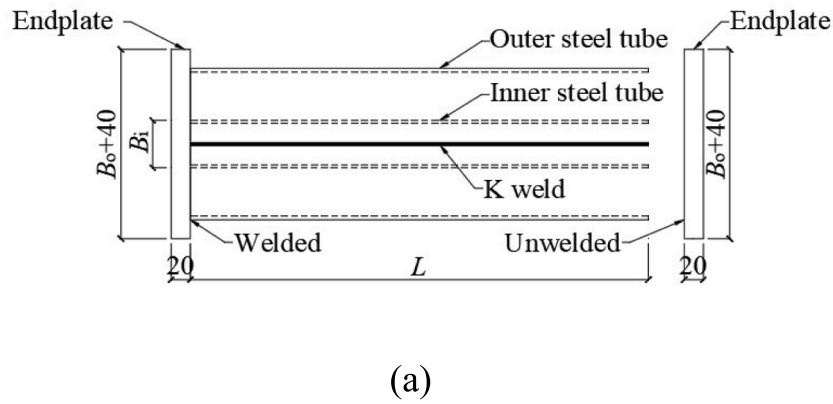

Fig. 6. Images of the CFDSST columns including (a) schematic of the layout (all units in mm) and (b) final specimens after preparation.

3. Test results and discussion

The test results are presented in tabulated form in Table 1, and are discussed in the following sub-sections. The table presents the ultimate load in each test $N_{\mathrm{ul,Exp}}$, as well as the ductility index *DI* and the strength index *SI*. The ductility index *DI* is determined as given in Eq. (2), which was proposed by Tao et al. [40]:

$$DI = \frac{\varepsilon_{85\%}}{\varepsilon_{75\%}/0.75} \tag{2}$$

where $\varepsilon_{85\%}$ is the axial strain corresponding to $0.85N_{\mathrm{ul,Exp}}$ in the descending response of the load-axial strain response, and $\varepsilon_{75\%}$ is the axial strain corresponding to $0.75N_{\mathrm{ul,Exp}}$ in the ascending response of the

load-axial strain curve. On the other hand, the strength index *SI* is calculated as given in Eq. (3):

$$SI = N_{\mathrm{ul}}/N_{\mathrm{ul,s}} \tag{3}$$

where N_{ul} represents the maximum axial load (either in the experiments, in which case it is equal to $N_{\mathrm{ul,Exp}}$, or through other means such as finite element analysis, as discussed later in this paper) and $N_{\mathrm{ul,s}}$ is determined as:

$$N_{\mathrm{ul,s}} = A_{\mathrm{sy,eff}}f_{\mathrm{yo}} + A_{\mathrm{ss}}f_{\mathrm{ys}} + A_{\mathrm{si}}f_{\mathrm{yi}} + A_{\mathrm{cs}}f_{\mathrm{cs}} + A_{\mathrm{ci}}f_{\mathrm{ci}} \tag{4}$$

In this expression, A_{ss}, A_{si}, A_{cs} and A_{ci} are the cross-sectional areas of the stiffeners, the inner steel tube, the sandwiched concrete and the core
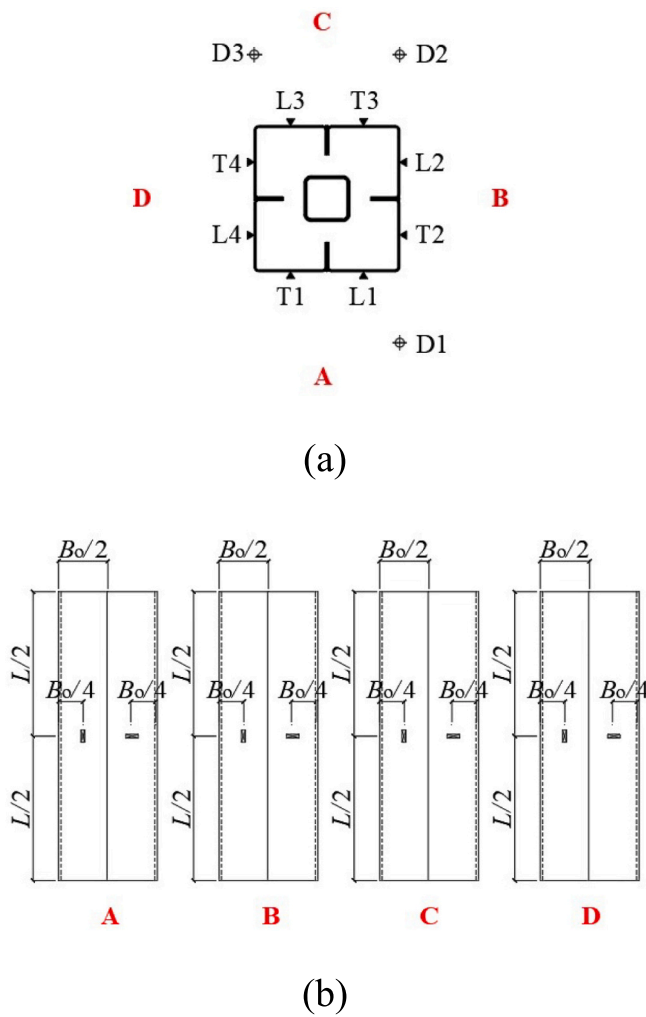
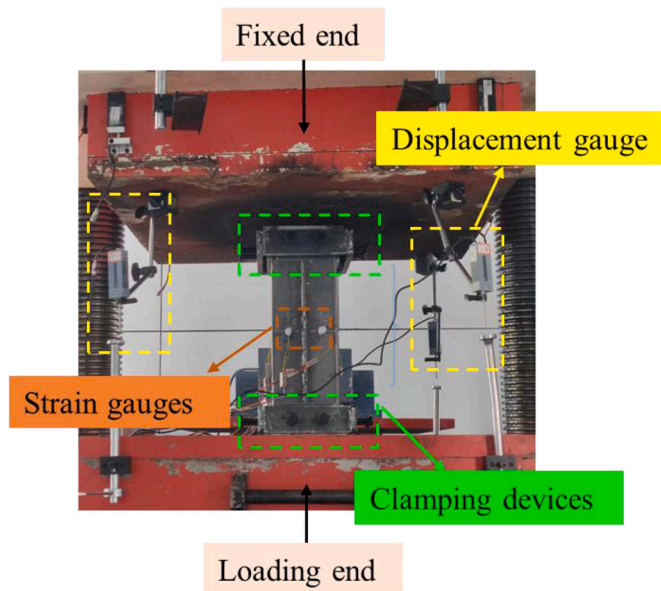**Fig. 7.** Locations of the strain gauges on the specimens including a (a) plan and (b) elevation view.

Fig. 8. Experimental test setup and clamping device.

concrete, respectively; f_{yo}, f_{ys} and f_{yi} are the yield strengths of the outer steel section, the stiffeners and the inner steel tube, respectively; and f_{cs} and f_{ci} are the compressive strengths of the sandwiched concrete and the core concrete, respectively. The relationship between the concrete compressive strength (f_{cs} and f_{ci}) and the concrete cube compressive strength (f_{cu}) is determined as given in Eq. (5):

$$f_{cs} \text{ or } f_{ci} = \left[0.76 + 0.2 log_{10} \left(\frac{f_{cu}}{19.6} \right) \right] f_{cu} \tag{5}$$

$A_{sy,eff}$ is the effective cross-sectional area of the outer steel tube as given in Eurocode 3 Part 1–1 [50] which accounts for local buckling which may take place in thin-walled steel tubes, and is given as:

$$A_{sy,eff} = \rho A_{so} \tag{6}$$

where ρ is the reduction factor for plate buckling, as defined in Eq. (7):

$$\rho = \begin{cases} 1.0 & \overline{\lambda}_p \leq 0.673 \\ \dfrac{\overline{\lambda}_p - 0.055(3 + \psi)}{\overline{\lambda}_p^{\,2}} \leq 1.0 & \overline{\lambda}_p > 0.673, \text{ where } (3 + \psi) \geq 0 \end{cases} \tag{7}$$

and ψ is the stress ratio which it is taken as unity for symmetrical cross-sections, while $\overline{\lambda}_p$ is given by Eq. (8):

$$\overline{\lambda}_p = \sqrt{\frac{f_{yo}}{\sigma_{cr}}} = \frac{B_o/2t_o}{28.4\varepsilon\sqrt{k_\sigma}} \tag{8}$$

In this expression, ε is taken as $\sqrt{\frac{235}{f_y}}$ and k_σ is taken as 4 when $\psi = 1$.

3.1. Ultimate loads and failure modes

The maximum loads carried by each specimen $N_{ul,Exp}$ is presented in Table 1. It is clear that the CFDSSTs generally reached greater loads compared with the CFSST and D-CFSST members. The strongest member of those examined was SS-180-3 which had the largest cross-section of those examined ($B_o = 180$ mm), was filled with concrete with a compressive strength of 70.30 MPa. Interestingly, this member did not necessarily contain steel sections with the highest yield strengths or thicknesses of those examined in this programme, and the concrete strength was clearly the most important material parameter in terms of the overall load-carrying capacity. This is explored in more detail later in this paper, together with an analysis of other important parameters to the overall load-displacement response.

The failure modes of all columns are shown in Fig. 9 and Fig. 10. It can be seen that all CFDSST columns failed due to local outward buckling of the outer steel tubes. However, although local buckling occurred at a number of locations along the columns length, as shown in the images, these did not occur in the same cross-section, which prevented the whole cross-section from failing with a sudden loss in load capacity. This may be a reason that the CFDSST columns had a greater post-failure bearing capacity compared with the CFSSTs or D-CFSST members. Additionally, no steel fracture was observed in the corner regions or welds of the test specimens. The prevention of corner fracture in particular, which may occur if the welds were in the corner regions, ensured good deformation capacity of the composite columns.

Additionally, it can be seen in Fig. 9 that local failure of the outer steel tube was more obvious with an increase in the concrete strength. This is because the higher strength concrete had less ductility and stiffness compared with lower strength concrete. Fig. 10 shows the failure modes of CFDSST columns with variation of t_o or B_i, and it can be seen that local failure of the outer steel tube was more obvious for members with a relatively thin outer tube and small width of the inner tube B_i. This phenomenon highlights that specimens that employed a relatively thick outer tube and large inner tube width had greater performance owing to the confinement provided to the sandwiched concrete.

SS-160-1   SS-160-2   SS-160-3

SS-180-1   SS-180-2   SS-180-3

Fig. 9. Failure modes of test CFDSST columns with varying concrete strengths f_c.

After testing, the outer steel tube was removed from the columns where possible to observe the failure modes in the sandwiched concrete; the images from a typical specimen are presented in Fig. 11(a). The crushing in the sandwiched concrete occurred largely at the buckling location of the outer steel tube. This is because there was no confinement after buckling of the outer steel tube. Additionally, the deformation of the inner square steel tube is shown in Fig. 11(b) and it is observed that there was no obvious deformation owing to the effective restraint provided by the outer and inner concrete. This ensured that the CFDSST columns had higher post-failure bearing capacity and energy absorption capacity compared with the CFSST and D-CFSST columns.

3.2. Axial load versus axial strain responses

Fig. 12 presents the outer steel strain distribution of typical specimens, where the symbols L and T are used to denote longitudinal strain and transverse strain, respectively, and negative and positive values of the strain readings denote compression and tension, respectively. From the Fig. 12, it is observed that the outer steel tube was fully under compression due to the negative longitudinal strains measured during the tests. Additionally, the strain developed slowly until the ultimate resistance was reached, and relatively low levels of deformation occurred in the outer steel tube until the ultimate resistance was achieved. On the descending branch of the response, after the peak values

were reached, the deformation of the outer steel tubes developed much more rapidly, especially in the transverse direction. This illustrates that the lateral confinement provided to the sandwiched concrete maximises after reaching the ultimate resistance.

3.3. Effect of the inner steel tube and core concrete

In order to comprehensively understand the behaviour of the CFDSST columns and their advantages, the effects of the inner steel tube and concrete are analysed in this section. Fig. 13(a) and (c) present a comparison of the CFDSST axial load-shortening responses with those from the CFSST and D-CFSST columns. The following observations are drawn from this comparison:

(1) In general, the axial load bearing capacity of CFDSST columns was higher than that of comparable CFSST and D-CFSST members. This is because the cross-section of the steel tube and concrete was higher than for CFSSTs and D-CFSSTs, respectively. This is further verified by examining Fig. 13(b) and (d) which present the normalised axial load *versus* axial shortening responses, whereby the loads on the y-axis are normalised against $N_{ul,s}$, as given in of Eq. (4).

(2) The residual bearing capacity of CFDSST columns was much higher than that of CFSST columns. Additionally, CFDSST columns showed better ductility than CFSST columns. This is also demonstrated in the normalised load graphs given in Fig. 13(b) and (d).

(3) The initial stiffness of CFDSST columns was greater than that of CFSST and D-CFSST columns.

3.4. Effect of concrete strength

The axial compressive behaviour of CFDSST columns with different concrete strengths is analysed in the current section. As observed in the axial load *versus* axial shortening results given in Fig. 14(a) and (c), the axial compressive bearing capacity of CFDSST columns tended to be greater for columns containing relatively higher strength concrete. Fig. 14(a) presents the data from group G3 as given in Table 1 and Fig. 14(c) presents the corresponding results for group G5. In these specimens the −1, −2 and − 3 terms of the designations represent members with f_{cu} values of 49.18 MPa, 53.58 MPa and 70.30 MPa, respectively. It is clear that the bearing capacity of the CFDSST columns increased by 32.5% for identical specimens with f_{cu} values which increased from 49.18 MPa (SS-160-1 and SS-180-1) to 70.30 MPa (SS-160-3 and SS-180-3). On the other hand however, the ductility of the same members was greatly reduced. This is evidenced by the ductility index (*DI*) as presented in Table 1, which reduced from 1.94 to 1.40 for SS-160-1 to SS-160-3, and from 2.02 to 1.29 for SS-180-1 to SS-180-3. With reference to Fig. 14(b) and (d), which present the normalised axial load *versus* axial shortening responses, similar conclusion can be drawn.

3.5. Ductility

In order to determine the effect of the inner steel tube on the ductility of the section, the ductility coefficient *DI* is used to evaluate the ductility of the columns, as presented in Table 1 and graphically presented in Fig. 15. It is observed by comparison of the *DI* for S-160 and SS-160-1, SS-160-4 and SS-160-6 that the ductility of the CFSST column S-160 was significantly improved by adding the inner steel tube to create the CFDSST sections. The same result was also observed for the columns with B_o = 180 mm. Additionally, the *DI* value decreased when the strength of the concrete increased, as previously discussed.

Fig. 10. Failure modes of test CFDSST columns with varying values of t_o or B.
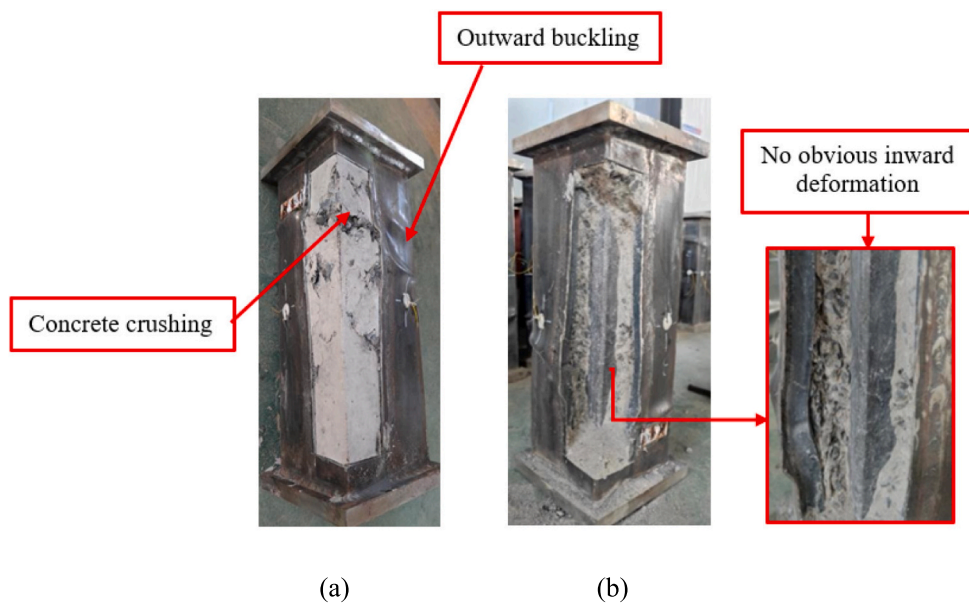

Fig. 11. Examination of the failure modes for a typical specimen including (a) concrete crushing and local buckling of the outer steel tube and (b) image of the inner steel tube with no obvious deformations.

(a) SS-160-2

(b) SS-160-4

(c) SS-180-2

(d) SS-180-6

(e) SS-180-7
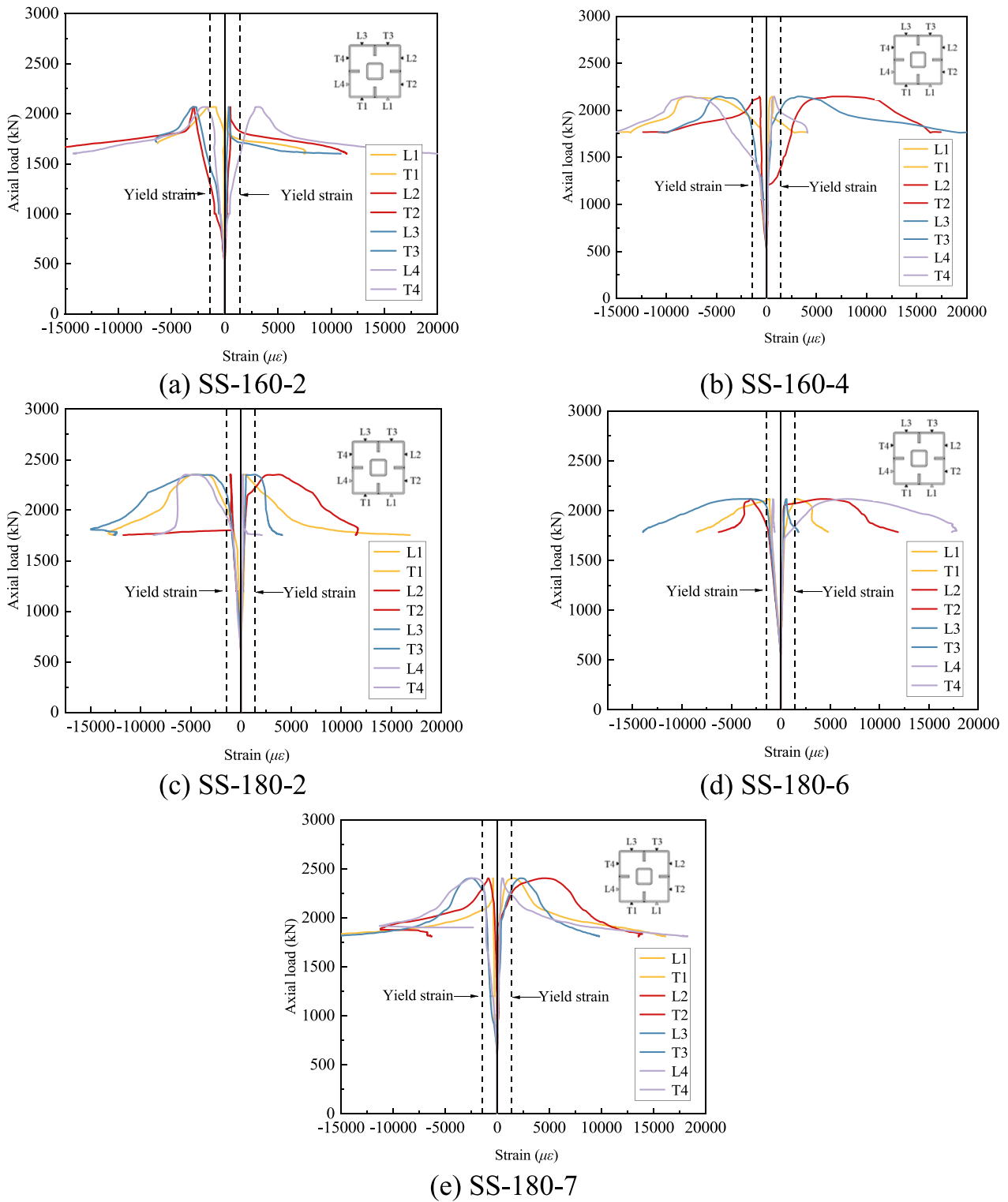
Fig. 12. Strain *versus* axial load responses for typical specimens.

3.6. Compressive strength

The axial compressive strength of CFDSSTs is made up of the sum of the five individual components which form part of the cross-section (*i.e.* the outer steel tube, inner steel tube, stiffeners, sandwiched concrete and core concrete) as well as any contribution made through composite action (*e.g.* additional strength in the concrete due to confinement). With reference to the data presented in Table 1, it is clear that the

concrete strength f_{cu} was a very influential property in terms of the overall load-carrying capacity, as well as the overall geometry. As stated before, all of the CFDSSTs resisted greater axial loads compared with the comparable CFSSTs and D-CFSST columns examined.

To evaluate the influence of the stiffeners and the inner steel tube on ultimate strength, as well as the effect of composite action on the overall load-carrying capacity, the strength index (*SI*) as given in Eq. (3) was determined for each test specimen and the results are presented in

(a) B_o=160 mm

(b) B_o=160 mm

(c) B_o=180 mm

(d) B_o=180 mm

Fig. 13. Comparison of the axial load *versus* axial shortening responses for CFDSST, CFSST and D-CFSST short columns.
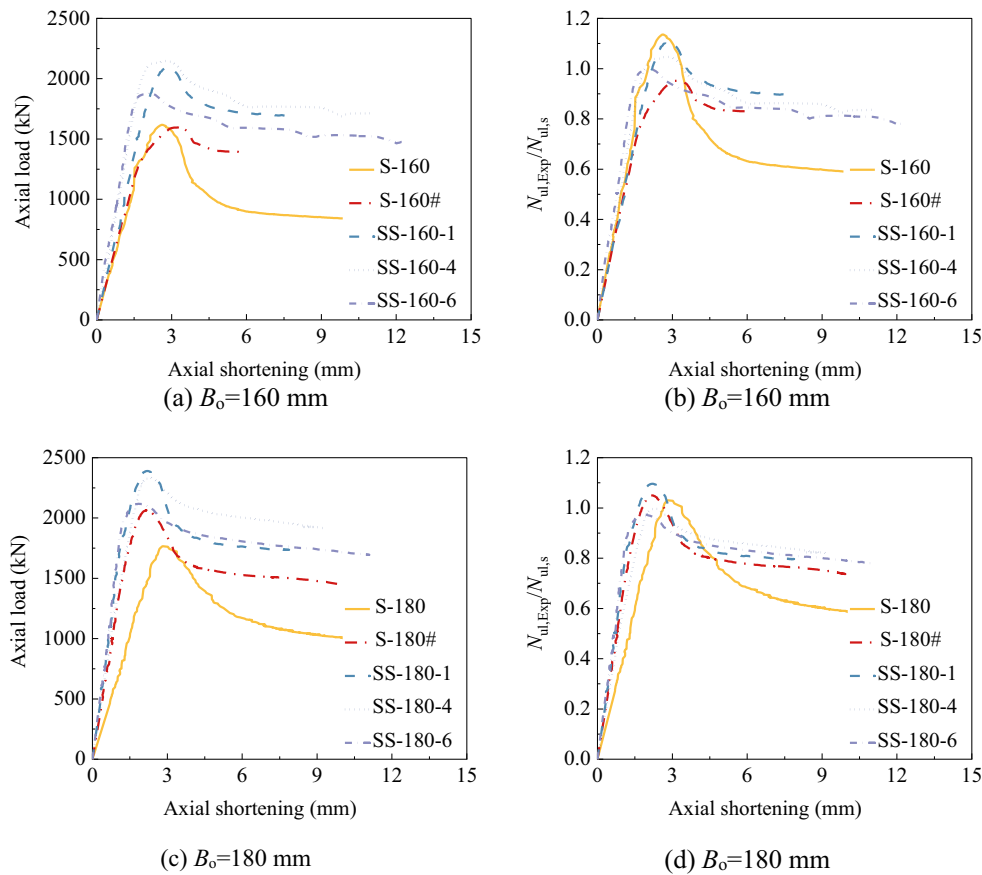
Table 1. For the fourteen CFDSST columns, the *SI* values range from 0.925 to 1.182 and the average *SI* value is 1.032. *SI* values which are greater than unity indicate that the composite action, largely through confinement of the sandwiched concrete, is playing a role in the load capacity. On the other hand, the average *SI* value for the two CFSST columns is 1.083 with a corresponding value of 1.001 for the two D-CFSST columns examined. From Table 1, it is observed that the *SI* value for specimens with a side width of 160 mm is generally greater than for those with a width of 180 mm. This indicates that there was greater confinement provided to the sandwiched concrete by the outer steel tube for the smaller specimens.

4. Finite element (FE) analysis

The experimental study was designed to understand the influence of some key parameters on the behaviour of CFDSSTs. This study is supplemented in the current section by the development of a finite element analysis model, which is validated against the test data and then employed to conduct a more detailed parametric study than was possible with the physical tests. The model was developed using the ABAQUS software [51] as described hereafter.

4.1. Description of the FE model

4.1.1. Initial model conditions

The numerical models were initially developed based on the material and geometrical properties of the test programme as described in Table 1. Fig. 16 presents schematic views of the FE columns and mesh. Both the sandwiched concrete and the concrete core were modelled using solid elements, known as C3D8R in the ABAQUS library, and the endplates were also simulated using C3D8R elements. On the other

hand, shell elements (S4R) were employed to simulate the outer and inner steel tubes; these were selected because they can capture local buckling modes in the steel tubes due to lateral expansion of the infilled concrete [52]. To ensure computational convergence of the model and to reduce the computational time without compromising the accuracy of the results, the overall element size was taken as $B_o/10$ following a mesh sensitivity study. The end conditions of the columns are as shown in Fig. 16, where reference points were located at the centre of both end-plates. Except for the axial direction displacement at the loading end (U_z), all other translational degrees of freedom (U_x and U_y at the top end and U_x, U_y and U_z at the bottom end) were restrained. Additionally, all rotational degrees of freedom (UR_x, UR_y and UR_z) at both ends of the column were restrained against movement. The columns were loaded in displacement control at the top of each member through the defined reference point.

The four lipped angles were restrained using a "tie" constraint between the contact faces of the stiffeners. Both endplates were set as rigid bodies and were effectively tied to the steel tube. A 'surface to surface contact' was defined at the interfaces between the concrete and steel elements and a 'hard contact' and 'penalty constraint algorithm' were selected to simulate the normal and tangential behaviour of the interactions between the interface of the steel tube and concrete as well as the interface of the concrete and the endplates. The bond and friction are important factors which influence the composite response. Liu et al. [43] studied the effect of the friction on axially loaded concrete filled steel tubular stub columns. It was shown that at the interface between the concrete and the steel tube, there was essentially no sliding between the two materials, indicating that the behaviour of CFST short columns is insensitive to the friction coefficient. In accordance with this study, the friction coefficient (μ) employed in the FE model developed herein for CFDSSTs was varied between 0.0 and 1.0 to explore its influence on the
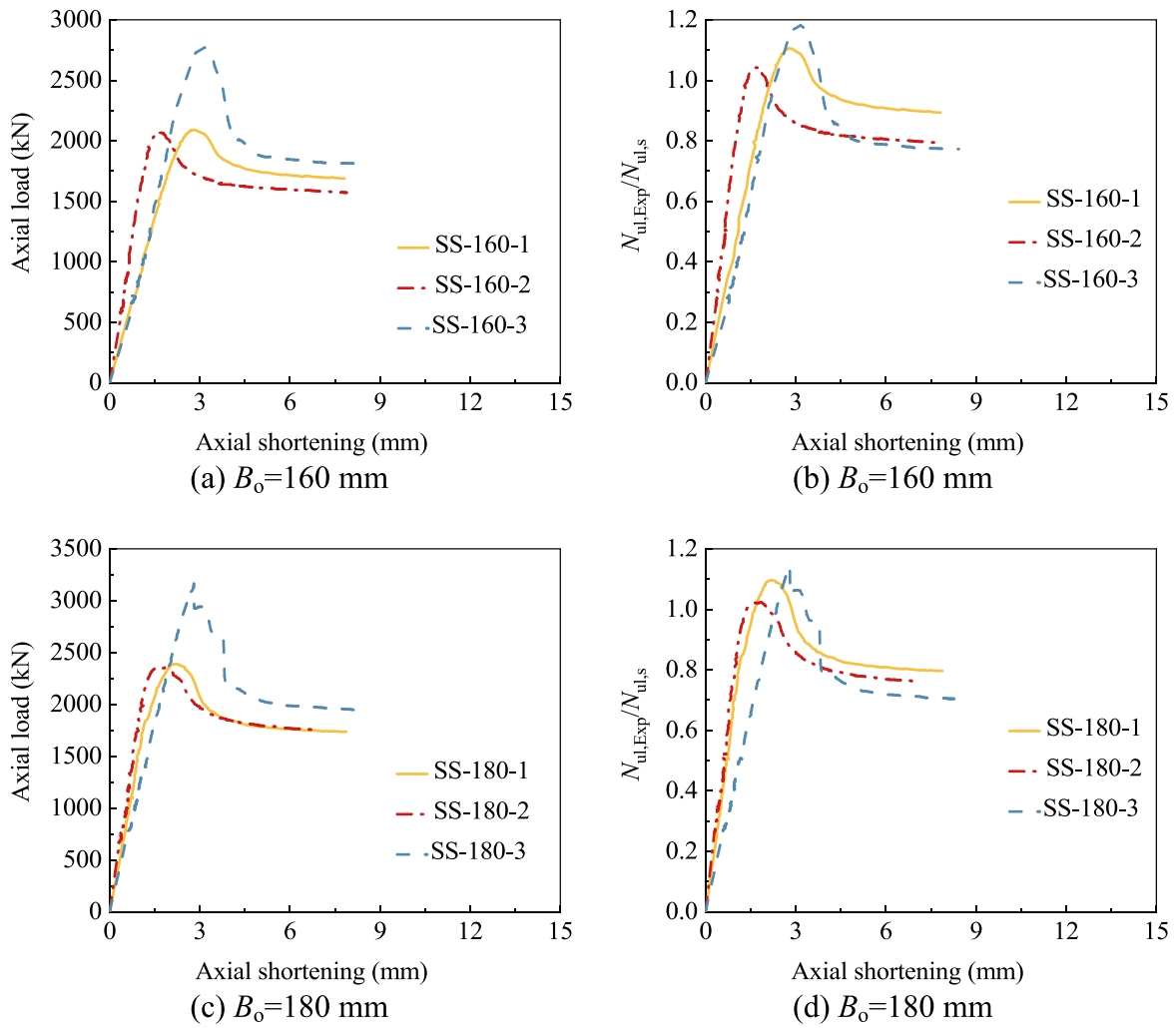
Fig. 14. Axial load-deformation curves of CFDSST columns with different concrete strengths.
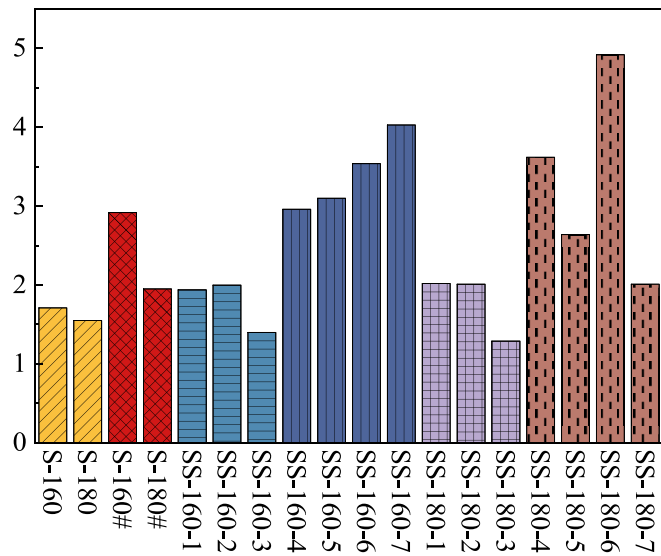
Fig. 15. Comparison of *DI* for test specimens.

Fig. 16. Schematic of the FE model including (a) overall view with applied load-displacement, (b) the steel elements and (c) the concrete elements.

axial capacity. The results for two of the specimens selected for illustration are presented in Table 3, where $N_{ul,FE}$ is the ultimate resistance obtained using the FE model. It is clear that μ has a negligible effect on

the results and therefore, the value of the friction coefficient was taken as 0.6 in this study as recommended by Liu et al. [43] and Han et al. [53].

Table 3
Effect of friction coefficient on the axial resistance of CFDSST columns.

Specimens	Ultimate resistance obtained by the FE model $N_{ul,FE}$ (kN)					
	$\mu = 0$	$\mu = 0.2$	$\mu = 0.4$	$\mu = 0.6$	$\mu = 0.8$	$\mu = 1.0$
SS-160-7	2180	2181	2180	2184	2169	2191
SS-180-7	2540	2537	2532	2534	2549	2544

4.1.2. Initial imperfections and residual stresses

Residual stresses develop in steel sections during the fabrication process, and may play a role in the performance of CFDSST columns. Previous studies show that tensile residual stresses σ_{rt} are typically near or equal to the material yield stress f_y [54] and the residual compressive stresses σ_{rc} are generally taken as $0.2f_y$ [55]. The idealized residual stress distribution 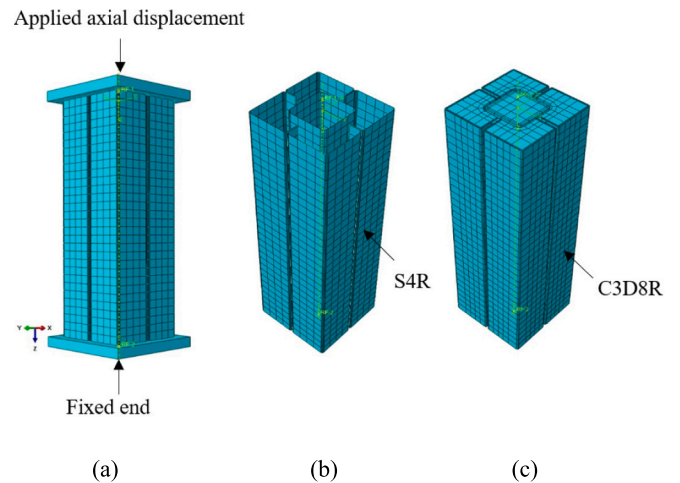adopted in the current study is shown in Fig. 17. The effect of residual stress on the axial load-deformation curve for specimen SS-160-1 (selected for illustration) is shown in Fig. 18. Although it is believed that residual stresses are influential to the behaviour of thin-walled hollow tubes, this effect is not significant for thin-walled concrete-filled composite columns, as most the column's strength is due to the concrete core [45].

The effects of initial imperfections on the axial resistance of thin-walled stiffened composite columns were analysed by Tao et al. [45]. Since short columns are not affected by global instability failure during loading, only local imperfections were considered in this study. The results demonstrate that although initial imperfections slightly reduce the overall capacity of composite columns, the influence is relatively small. Hence, the effect of initial imperfections and residual stresses on the ultimate resistance of CFDSST columns was neglected in the current study. It is noteworthy that similar conclusions were also determined elsewhere [56], when only axial compression behaviour was considered as in the current paper.

4.1.3. Material modelling

In this sub-section, the simulation of both the steel components and the concrete infill is described. All of the steel in the CFDSSTs is modelled using an identical material model, and this is also true for the concrete. For the steel sections, it is widely accepted that local buckling is more likely in square hollow sections compared with circular hollow sections, and also the benefits of concrete confinement can be less effective. Therefore, square CFST columns seldom demonstrate significant levels of strain hardening as they typically remain within the elastic region of the response [46]. Hence, in the current analysis of CFDSSTs, an elastic-perfectly plastic material model was employed to simulate the steel material in both the inner and outer steel tubes. Additionally, to accurately describe the change in cross-sectional area, the true stress (σ_{true}) and logarithmic plastic true strain (ε_{true}) values were employed. These were calculated in accordance with Eqs. (9) and (10), respectively:

$$\sigma_{true} = \sigma \cdot (1 + \varepsilon) \tag{9}$$

$$\varepsilon_{true} = ln(1 + \varepsilon) - \frac{\sigma_{true}}{E} \tag{10}$$

where σ and ε are the engineering stress and strain, respectively.
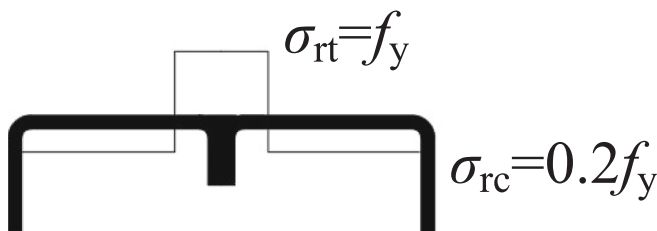
Fig. 17. Distribution of residual stresses in the outer section.
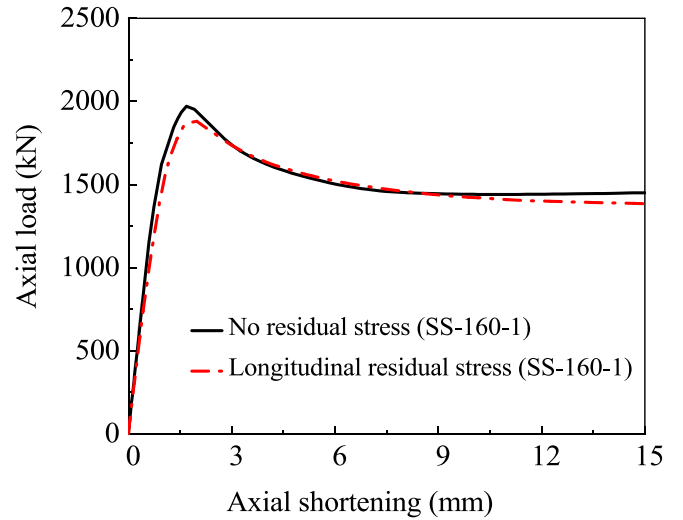
Fig. 18. Axial load-lateral deformation for CFDSSTs with and without residual stress.

For the sandwiched and core concrete, the commonly-used concrete damage plasticity (CDP) model in the ABAQUS library was employed. The stress-strain response for concrete proposed by Tao et al. [46] which accounts for confinement due to the steel tubes, was adopted, and this is presented in Fig. 19. It is observed that for confined concrete, the plateau stage from point A to point B reflects an increase in peak strain which occurs due to confinement. The strength increase due to confinement was captured in the simulation through the interaction between the steel sections and the concrete. The concrete constitutive relationship proposed by Tao et al. [46] and adopted in the FE model is expressed in Eq. (11):

$$\sigma = \begin{cases} \dfrac{AX + BX^2}{1 + (A - 2)X + (B + 1)X^2}f_c & 0 < \varepsilon \leq \varepsilon_{c0} \\ f_c & \varepsilon_{c0} < \varepsilon \leq \varepsilon_{cc} \\ f_r + (f_c - f_r)exp\left[-\left(\dfrac{\varepsilon - \varepsilon_{cc}}{\alpha}\right)^\beta\right] & \varepsilon \geq \varepsilon_{cc} \end{cases} \tag{11}$$

in which $X = \varepsilon/\varepsilon_{c0}$, $A = (E_c\varepsilon_{c0})/f_c$, $B = \left((A - 1)^2/0.55\right) - 1.0$ and E_c is taken as $4700\sqrt{f_c}$, and these terms are defined as given in Fig. 19. The residual stress f_r is taken as $0.1f_c$. The parameter α is determined in
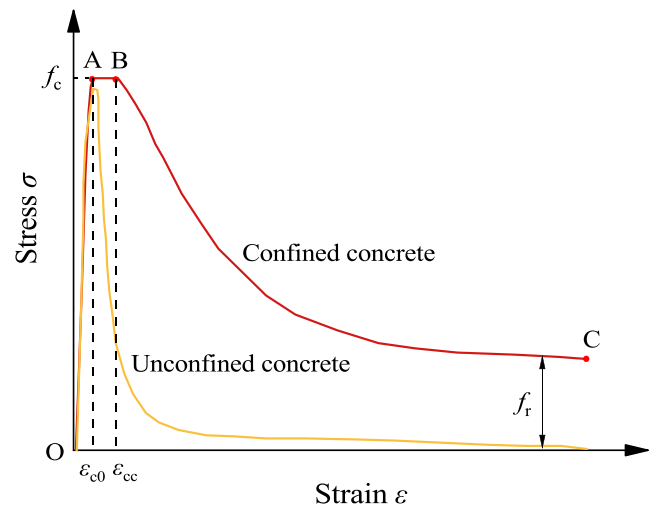
Fig. 19. Unconfined and confined stress-strain (σ-ε) responses of concrete.

accordance with Eq. (12) and β is taken as 0.92. The strain values at point A (ε_{c0}) and at point B (ε_{cc}) were determined by Eqs. (13) and (14), respectively.

$$\alpha = 0.005 + 0.0075\xi_c \tag{12}$$

$$\varepsilon_{c0} = 0.00076 + \sqrt{(0.626f_c - 4.33) \times 10^{-7}} \tag{13}$$

$$\frac{\varepsilon_{cc}}{\varepsilon_{c0}} = e^k, \quad k = \left(2.9224 - 0.00367f_c'\right)\left(\frac{f_B}{f_c}\right)^{0.3124+0.002f_c} \tag{14}$$

where f_B was proposed by Tao et al. [46] based on a regression analysis, and as expressed as:

$$f_B = \frac{0.25 \cdot \left(1 + 0.027f_y\right) \cdot e^{-0.02\sqrt{B^2+D^2}}}{1 + 1.6e^{-10} \cdot (f_c)^{4.8}} \tag{15}$$

The confinement factor ξ_c is a crucial parameter for composite columns, and is expressed as:

$$\xi_c = \frac{A_s f_y}{A_c f_{ck}} \tag{16}$$
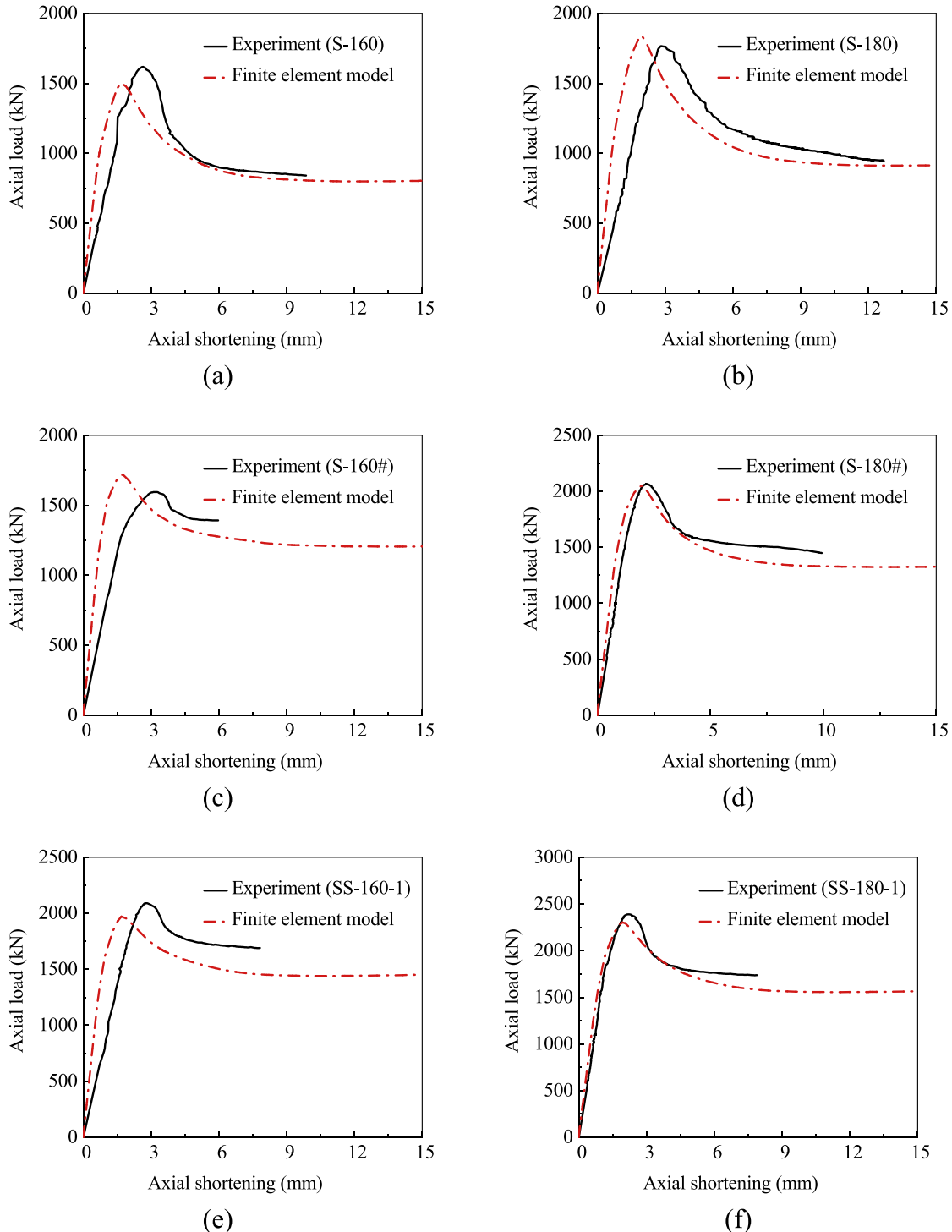
Fig. 20. Comparison between FE and experimental axial load-displacement responses of test specimens.
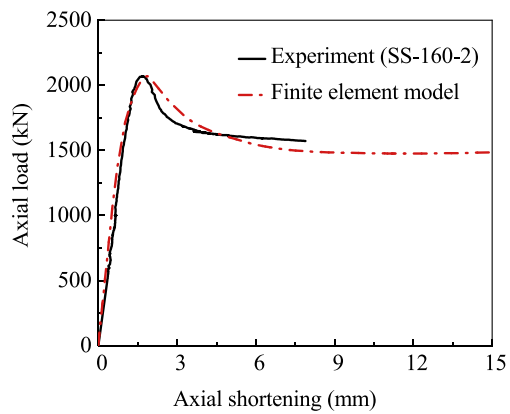
(g)
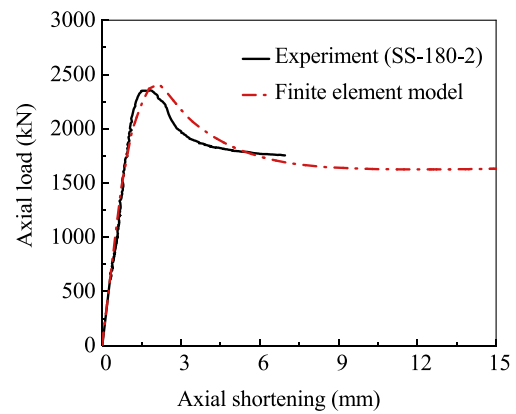
(h)
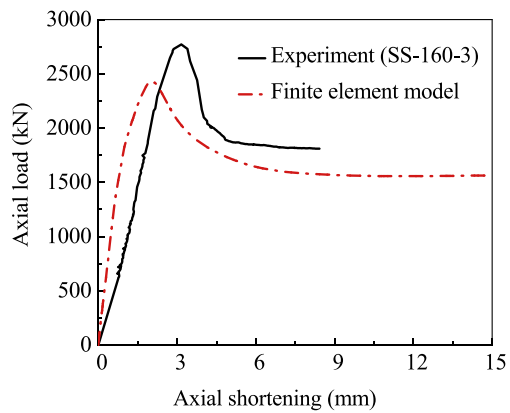
(i)
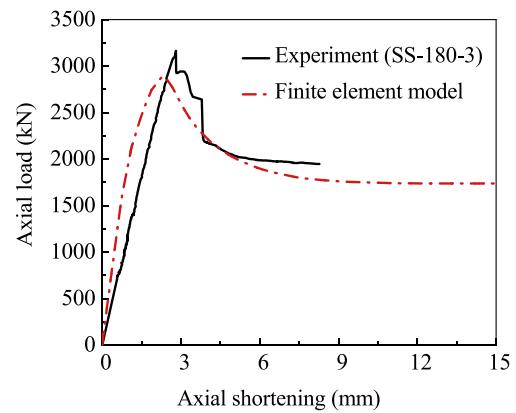
(j)
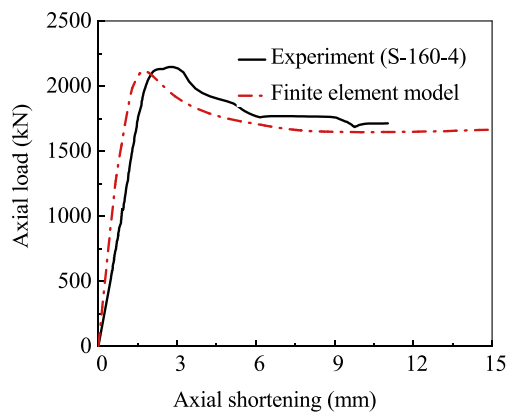
(k)

(l)

Fig. 20. (*continued*).

(m)

(n)

(o)

(p)

(q)

(r)
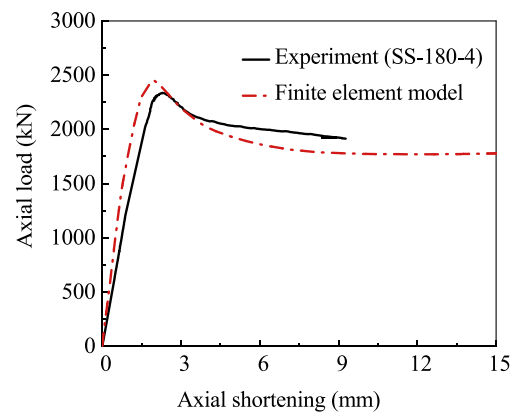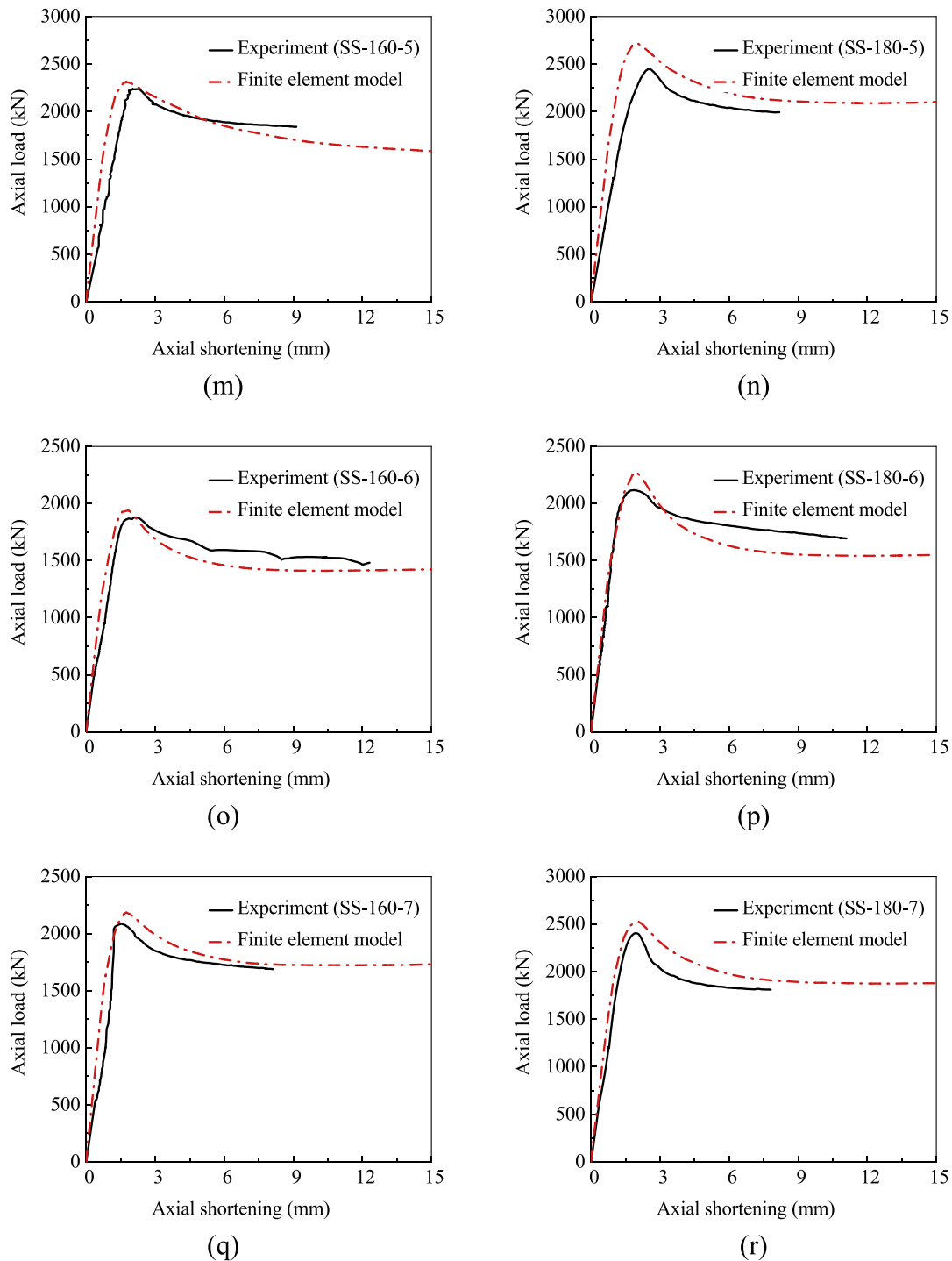
Fig. 20. (*continued*).

where A_s and A_c are the cross-sectional areas of the steel tube and infill concrete, respectively, and f_y and f_{ck} are the characteristic design strengths of the two component materials, respectively, and f_{ck} was taken as 0.67 f_{cu}. To simplify the calculation, the stiffeners were not considered when determining A_s and A_c as suggested by Wang et al. [32].

4.2. Validation of the FE model

The accuracy of the FE model for predicting the response of CFDSST columns was assessed by comparing the results with the experimental values described earlier in this paper. The ultimate resistances predicted by the model $N_{ul,FE}$ are listed in Table 1, together with the corresponding experimental values $N_{ul,Exp}$, and the $N_{ul,FE}/N_{ul,Exp}$ ratios. With a mean $N_{ul,FE}/N_{ul,Exp}$ value of 1.008 and a coefficient of variation (COV) value of 0.064, it is observed that the proposed FE model provides an accurate prediction of the ultimate resistance of CFDSST short columns.

For further validation, a comparison of the experimental and predicted axial load *versus* displacement responses is presented in Fig. 20. Overall, it is shown that the FE model is able to provide a good depiction of the response. There are some discrepancies, which are attributed to the idealisation of the material properties and boundary conditions in

Table 4
Details of the parametric study on UHS-CFDDST slender columns.

Groups	Specimens	B_o (mm)	t_o (mm)	f_{yo} (MPa)	f_{cs} (MPa)	B_o/t_o	h_s (mm)	B_i (mm)	t_i (mm)	f_{yi} (MPa)	f_{ci} (MPa)	B_i/t_i	B_i/B_o	$N_{ul,FE}$ (kN)	N_s (kN)	SI
G1	S1	200	2	235	40	100.0	30	80	3.0	355	40	26.7	0.40	2365	2233	1.06
	S2	200	2	355	40	100.0	30	80	3.0	355	40	26.7	0.40	2609	2384	1.09
	S3	200	2	420	40	100.0	30	80	3.0	355	40	26.7	0.40	2729	2460	1.11
	S4	200	2	550	40	100.0	30	80	3.0	355	40	26.7	0.40	3005	2601	1.16
	S5	200	2	235	60	100.0	30	80	3.0	355	40	26.7	0.40	3005	2864	1.05
	S6	200	2	235	80	100.0	30	80	3.0	355	40	26.7	0.40	3587	3496	1.03
	S7	200	2	235	100	100.0	30	80	3.0	355	40	26.7	0.40	4235	4127	1.03
	S8	200	2	235	130	100.0	30	80	3.0	355	40	26.7	0.40	5106	5074	1.01
	S9	200	2	235	40	100.0	30	80	3.0	235	40	26.7	0.40	2249	2122	1.06
	S10	200	2	235	40	100.0	30	80	3.0	420	40	26.7	0.40	2425	2293	1.06
	S11	200	2	235	40	100.0	30	80	3.0	550	40	26.7	0.40	2569	2413	1.06
	S12	200	2	235	40	100.0	30	80	3.0	355	60	26.7	0.40	2465	2342	1.05
	S13	200	2	235	40	100.0	30	80	3.0	355	80	26.7	0.40	2538	2452	1.04
	S14	200	2	235	40	100.0	30	80	3.0	355	100	26.7	0.40	2601	2561	1.02
	S15	200	2	235	40	100.0	30	80	3.0	355	130	26.7	0.40	2687	2726	0.99
	S16	200	2	235	40	100.0	25	80	3.0	355	40	26.7	0.40	2371	2217	1.07
	S17	200	2	235	40	100.0	40	80	3.0	355	40	26.7	0.40	2427	2264	1.07
	S18	200	2	235	40	100.0	50	80	3.0	355	40	26.7	0.40	2456	2295	1.07
	S19	200	2	235	40	100.0	30	60	3.0	355	40	20.0	0.30	2305	2157	1.07
	S20	200	2	235	40	100.0	30	100	3.0	355	40	33.3	0.50	2464	2308	1.07
	S21	200	2	235	40	100.0	30	120	3.0	355	40	40.0	0.60	2495	2384	1.05
	S22	200	2.5	235	40	80.0	30	80	3.0	355	40	26.7	0.40	2460	2373	1.04
	S23	200	3	235	40	66.7	30	80	3.0	355	40	26.7	0.40	2556	2478	1.03
	S24	200	2	235	40	100.0	30	80	2.0	355	40	40.0	0.40	2254	2138	1.05
	S25	200	2	235	40	100.0	30	80	4.0	355	40	20.0	0.40	2439	2325	1.05
G2	S26	280	2	235	40	140.0	40	80	3.0	355	40	26.7	0.29	4091	3806	1.07
	S27	280	2	355	40	140.0	40	80	3.0	355	40	26.7	0.29	4331	3978	1.09
	S28	280	2	420	40	140.0	40	80	3.0	355	40	26.7	0.29	4510	4064	1.11
	S29	280	2	550	40	140.0	40	80	3.0	355	40	26.7	0.29	4878	4226	1.15
	S30	280	2	235	60	140.0	40	80	3.0	355	40	26.7	0.29	5451	5190	1.05
	S31	280	2	235	80	140.0	40	80	3.0	355	40	26.7	0.29	6787	6573	1.03
	S32	280	2	235	100	140.0	40	80	3.0	355	40	26.7	0.29	8197	7956	1.03
	S33	280	2	235	130	140.0	40	80	3.0	355	40	26.7	0.29	10,180	10,031	1.01
	S34	280	2	235	40	140.0	40	80	3.0	235	40	26.7	0.29	3971	3695	1.07
	S35	280	2	235	40	140.0	40	80	3.0	420	40	26.7	0.29	4153	3866	1.07
	S36	280	2	235	40	140.0	40	80	3.0	550	40	26.7	0.29	4267	3986	1.07
	S37	280	2	235	40	140.0	40	80	3.0	355	60	26.7	0.29	4173	3916	1.07
	S38	280	2	235	40	140.0	40	80	3.0	355	80	26.7	0.29	4219	4025	1.05
	S39	280	2	235	40	140.0	40	80	3.0	355	100	26.7	0.29	4250	4135	1.03
	S40	280	2	235	40	140.0	40	80	3.0	355	130	26.7	0.29	4366	4299	1.02
	S41	280	2	235	40	140.0	30	80	3.0	355	40	26.7	0.29	4045	3775	1.07
	S42	280	2	235	40	140.0	50	80	3.0	355	40	26.7	0.29	4122	3837	1.07
	S43	280	2	235	40	140.0	70	80	3.0	355	40	26.7	0.29	4181	3900	1.07
	S44	280	2	235	40	140.0	40	60	3.0	355	40	20.0	0.21	4007	3731	1.07
	S45	280	2	235	40	140.0	40	120	3.0	355	40	40.0	0.43	4223	3957	1.07
	S46	280	2	235	40	140.0	40	160	3.0	355	40	53.3	0.57	4379	4109	1.07
	S47	280	2.5	235	40	112.0	40	80	3.0	355	40	26.7	0.29	4235	3977	1.06
	S48	280	3	235	40	93.3	40	80	3.0	355	40	26.7	0.29	4359	4164	1.05
	S49	280	2	235	40	140.0	40	80	2.0	355	40	40.0	0.29	3991	3712	1.08
	S50	280	2	235	40	140.0	40	80	4.0	355	40	20.0	0.29	4174	3898	1.07
G3	S51	400	2	235	40	200.0	70	80	3.0	355	40	26.7	0.20	7625	7150	1.07
	S52	400	2	355	40	200.0	70	80	3.0	355	40	26.7	0.20	8148	7379	1.10
	S53	400	2	420	40	200.0	70	80	3.0	355	40	26.7	0.20	8407	7496	1.12
	S54	400	2	550	40	200.0	70	80	3.0	355	40	26.7	0.20	8898	7721	1.15
	S55	400	2	235	60	200.0	70	80	3.0	355	40	26.7	0.20	10,467	10,136	1.03
	S56	400	2	235	80	200.0	70	80	3.0	355	40	26.7	0.20	13,505	13,123	1.03
	S57	400	2	235	100	200.0	70	80	3.0	355	40	26.7	0.20	16,536	16,109	1.03
	S58	400	2	235	130	200.0	70	80	3.0	355	40	26.7	0.20	20,990	20,589	1.02
	S59	400	2	235	40	200.0	70	80	3.0	235	40	26.7	0.20	7501	7039	1.07
	S60	400	2	235	40	200.0	70	80	3.0	420	40	26.7	0.20	7703	7210	1.07
	S61	400	2	235	40	200.0	70	80	3.0	550	40	26.7	0.20	7822	7330	1.07
	S62	400	2	235	40	200.0	70	80	3.0	355	60	26.7	0.20	7741	7259	1.07
	S63	400	2	235	40	200.0	70	80	3.0	355	80	26.7	0.20	7789	7369	1.06
	S64	400	2	235	40	200.0	70	80	3.0	355	100	26.7	0.20	7851	7478	1.05
	S65	400	2	235	40	200.0	70	80	3.0	355	130	26.7	0.20	7924	7642	1.04
	S66	400	2	235	40	200.0	30	80	3.0	355	40	26.7	0.20	7505	7025	1.07
	S67	400	2	235	40	200.0	50	80	3.0	355	40	26.7	0.20	7488	7087	1.06
	S68	400	2	235	40	200.0	90	80	3.0	355	40	26.7	0.20	7685	7212	1.07
	S69	400	2	235	40	200.0	70	120	3.0	355	40	40.0	0.30	7817	7301	1.07
	S70	400	2	235	40	200.0	70	160	3.0	355	40	53.3	0.40	7942	7452	1.07
	S71	400	2	235	40	200.0	70	220	3.0	355	40	73.3	0.55	8179	7679	1.07
	S72	400	2.5	235	40	160.0	70	80	3.0	355	40	26.7	0.20	7866	7357	1.07
	S73	400	3	235	40	133.3	70	80	3.0	355	40	26.7	0.20	8092	7592	1.07
	S74	400	2	235	40	200.0	70	80	2.0	355	40	40.0	0.20	7426	7055	1.05
	S75	400	2	235	40	200.0	70	80	4.0	355	40	20.0	0.20	7745	7242	1.07

the FE model. The model is not able to capture an unknown or random material defects, slip at the supports and loading, or voltage interferences in the strain gauge measurements, for example. Nevertheless, the comparisons are reasonable and it is clear that the FE model captures the main behavioural trends including stiffening behaviour, peak loads and displacements and also the softening responses.

5. Parametric analysis

The validated FE model was employed to conduct a detailed parametric study, so that the key influential properties could be carefully examined. The variables examined included the yield strength of the outer and inner steel tubes, the strength of the sandwiched concrete and the core concrete, the depth of the stiffeners, the diameter-to-width ratio of the outer and inner steel tubes, and the hollow ratio χ. A total of 75 models were simulated, and these are divided herein into three different groups according to different B_o values. The details and ultimate resistances obtained by the FE models of CFDSST columns are given in Table 4. Unless otherwise stated, the benchmark properties for the specimens examined are as follows: the yield strength and thickness of the outer section are taken as $f_{yo} = 235$ MPa and $t_o = 2$ mm, respectively; the concrete in both the sandwiched and core regions (f_{cs} and f_{ci}) has a compressive strength of 40 MPa; the width, thickness and yield strength of the inner steel section are $B_i = 80$ mm, $t_i = 3$ mm and $f_{yi} = 355$ MPa; and the height of the stiffeners h_s is 30 mm.

5.1. Steel strength

The influence of steel yield strength of the outer and inner steel tubes on the behaviour of CFDSST columns was investigated by varying the grade of steel in the FE model. Four different yield strengths were examined, including 235, 355, 420 and 550 MPa. Note that despite the steel and concrete material strengths of columns S4, S11, S29, S36, S54, S61 are not compatible according to Liew et al. [57], they have been checked. The results are presented in Figs. 21 and 22. It is observed that increasing the yield strength of the outer tube leads to a corresponding increase in the ultimate strength of CFDSST columns and an improvement in the ductility and stiffness of CFDSST columns. On the other hand, the behaviour and ultimate resistance of CFDSST columns were not greatly affected by increasing of the yield strength of the inner tube. Additionally, from Fig. 23, it can be seen that as the outer tube width increases, the ductility and post-failure bearing capacity decrease quite clearly. This is because the lateral confinement of the filled concrete

reduces as the width of the outer tube increases, which is in agreement with previous research findings [10,11]. With reference to Fig. 22(b) and (d), which present the normalised load *versus* axial shortening responses, it is observed that the behaviour of all the specimens is quite similar. The initial stiffness tends to increase with a reduction of B_o, irrespective of the steel strength. Additionally, as in all cases, the normalised ultimate load is greater than unity, it is demonstrated that confirms the composite action in CFDSST columns is effective for strengthening the columns. It is also observed that the initial stiffness does not change for members made using hollow sections with different steel strengths.

5.2. Concrete strength

A range of different concrete values were examined, from normal strength concrete (NSC) with a compressive strength of 40 MPa, to ultra-high strength concrete (UHSC) with a maximum compressive strength of 130 MPa. The concrete classification is based on the guidance given in Eurocode 2 Part 1–1 [58]. The results are presented in Figs. 23 and 24. It is clear that the influence of the sandwiched concrete between the two steel tubes is significant, with increased strength resulting in a corresponding improvement to the ultimate resistance of the column. On the other hand, the strength of the core concrete within the inner steel tube is significantly less influential to both the peak capacity as well as the overall behaviour. Additionally, as the width of the outer steel tube increases, the relative benefit of employing higher strength concrete in the sandwich region is even greater. This is because the concrete component of composite columns bears most of the compressive load under normal structural conditions, and the cross-sectional area of sandwiched concrete is larger as the width of the outer steel tube increases. With reference to the normalised axial load *versus* axial shortening graphs presented in Fig. 24(b), it is observed that the initial stiffness increases with a reduction in the cross-sectional width and the sandwiched concrete strength. Additionally, the normalised ultimate load is greater than unity in all cases, confirming the positive contribution made by composite action for these columns. Furthermore, as shown in Fig. 24(d), the effect of the core concrete strength on the normalised load *versus* axial shortening behaviour is negligible.

5.3. Stiffener depth h_s

The depth of the stiffeners employed in the outer steel tubes was varied in the FE model. The minimum values examined were calculated
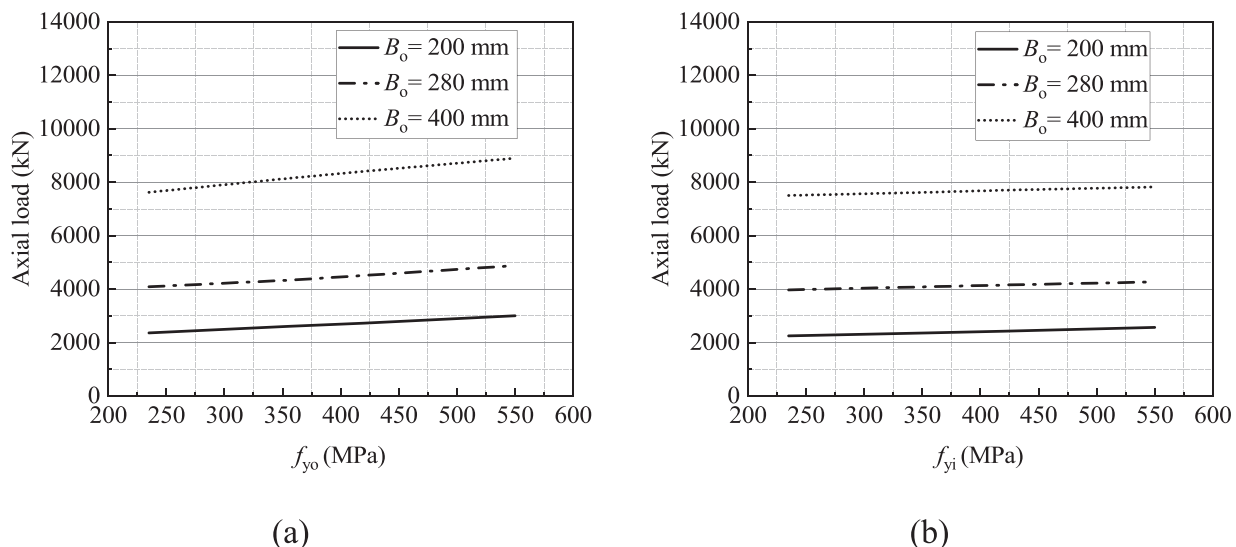

Fig. 21. Influence of different yield strengths for (a) the outer tube and (b) the inner tube, on the ultimate resistance of CFDSST columns.
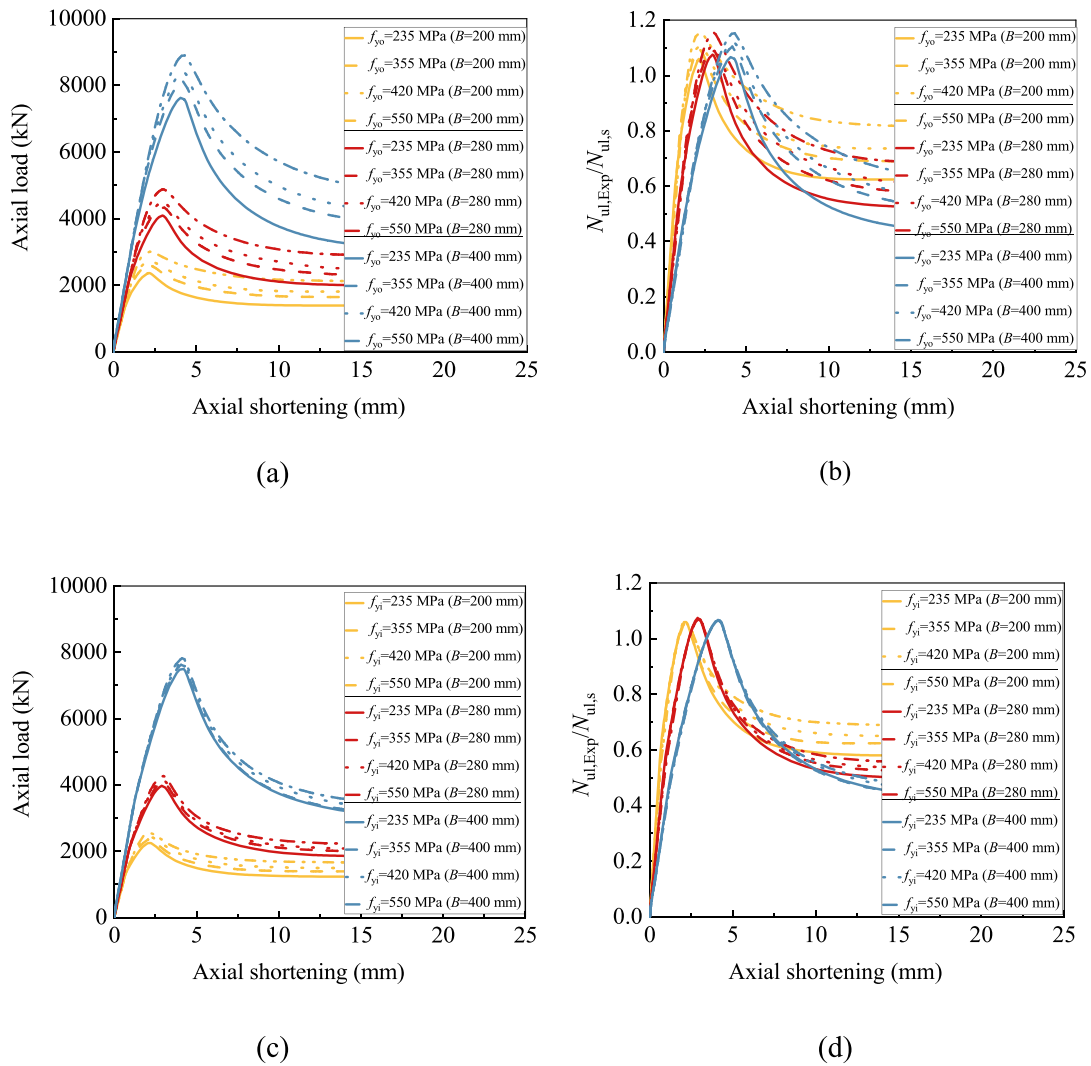
Fig. 22. Influence of different yield strengths for (a and b) the outer tube and (c and d) the inner tube, on the axial load *versus* displacement responses of CFDSST columns.
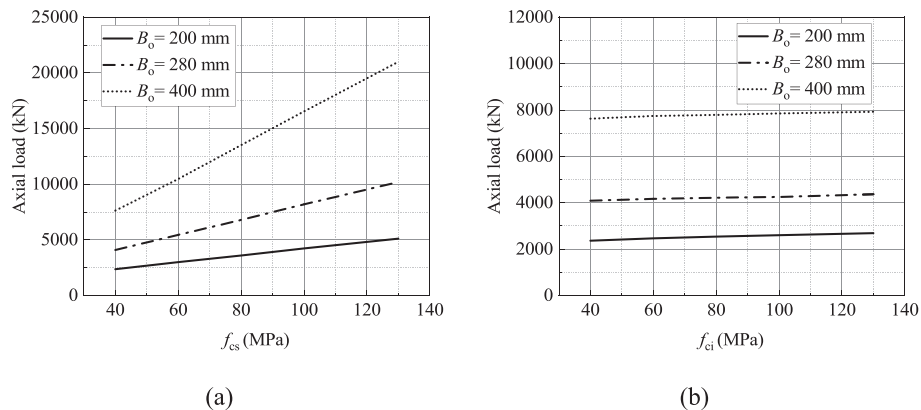
Fig. 23. Influence of different concrete strengths for (a) the sandwiched concrete and (b) the core concrete, on the ultimate resistance of CFDSST columns.

in accordance with the guidance proposed by Tao et al. [40], and reasonable maximum values were adopted based on engineering judgement. Accordingly, the range of values of stiffener depth examined for specimens with $B_o = 200$ mm was between 22.3 and 50 mm, for those with $B_o = 280$ mm, was 33 to 70 mm, and when $B_o = 400$ mm, h_s was varied between 50 and 90 mm. Fig. 25 illustrates the relationships

between $N_{ul,FE}$ and h_s. It is observed that the capacity was only slightly affected by changing the stiffeners depth and it is concluded that the increasing depth of stiffeners has little effect on the resistance of CFDSST columns.

(a)

(b)

(c)

(d)
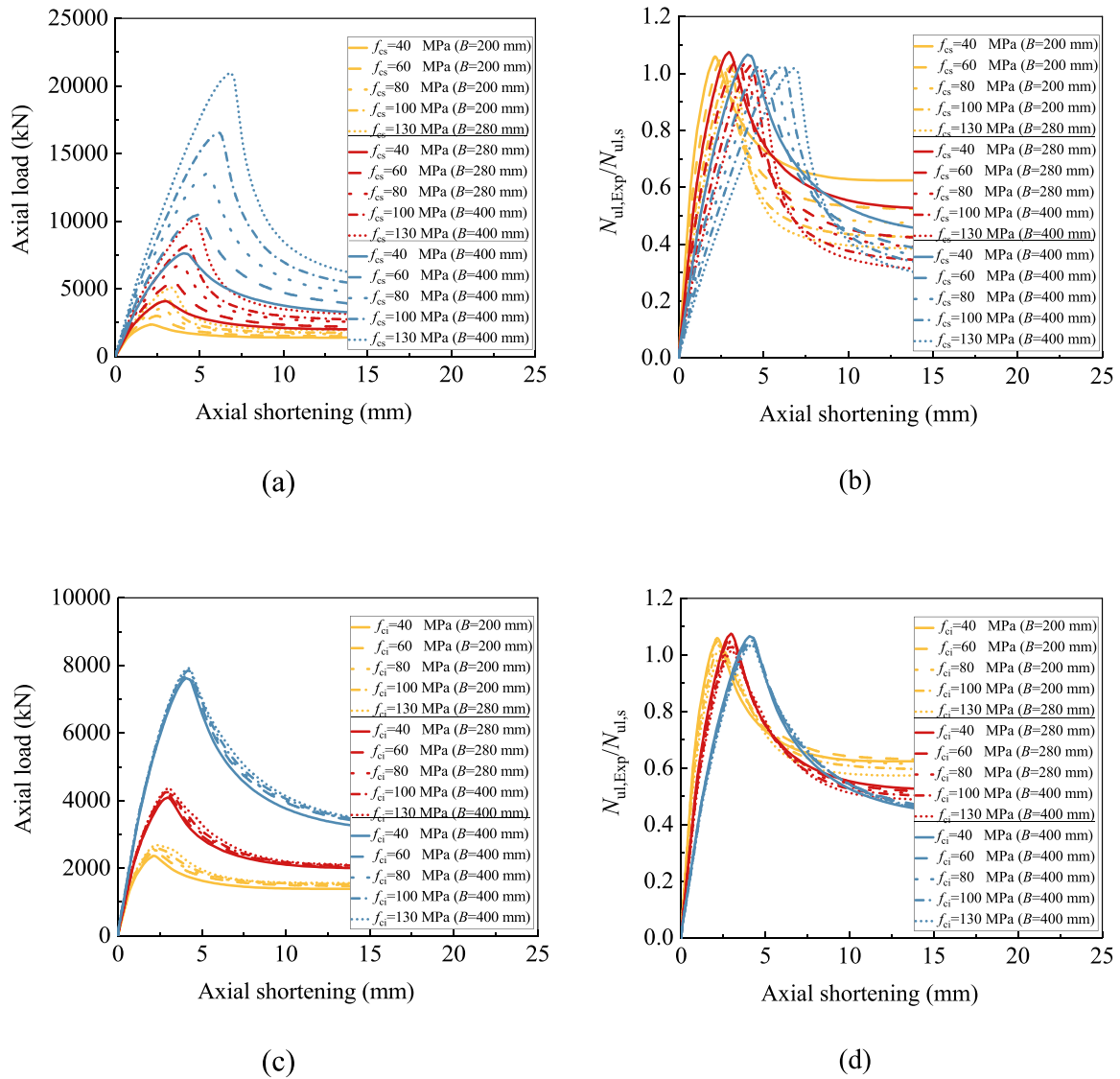
Fig. 24. Influence of different concrete strengths for (a and b) the sandwiched concrete and (c and d) the core concrete.
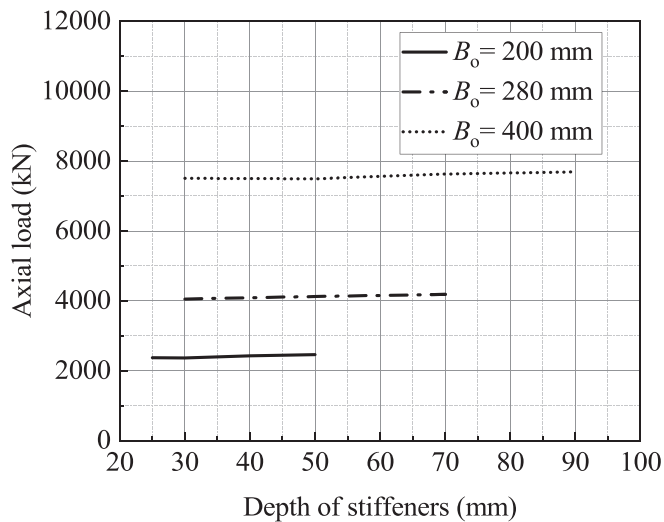
Fig. 25. Influence of stiffener depth on the resistance of CFDSST columns.

5.4. B_o/t_o and B_i/t_i ratios

Figs. 26 and 27 present the influence that the width-to-thickness ratio of the outer steel tube (B_o/t_o) and the inner steel tube (B_i/t_i) has on the behaviour and resistance of CFDSST columns. From Fig. 26(a) and Fig. 27(a), it is observed that the ultimate resistance, ductility and post-failure bearing resistance of CFDSST columns reduces as the B_o/t_o ratio increases. This is due to the reduction in the confining stress of the concrete and the increased possibility of local buckling in the steel tubes. From Fig. 26(b) and Fig. 27(c), it is shown that the ultimate resistance of the columns only slightly reduces with an increase of the B_i/t_i ratio and this is generally a quite uninfluential parameter to the behaviour. This is because of the constraint effect of the concrete to the inner circular tube from both sides that prevent it from buckling locally. With reference to Fig. 26(b) and (d), it is observed that the initial stiffness tends to increase with a reduction in the cross-sectional width irrespective of B_o/t_o and B_i/t_i.

5.5. Hollow ratio χ

The hollow ratio χ in the current study is defined as the ratio of the width of the inner steel tube to that of the outer steel tube (*i.e.* B_i/B_o).
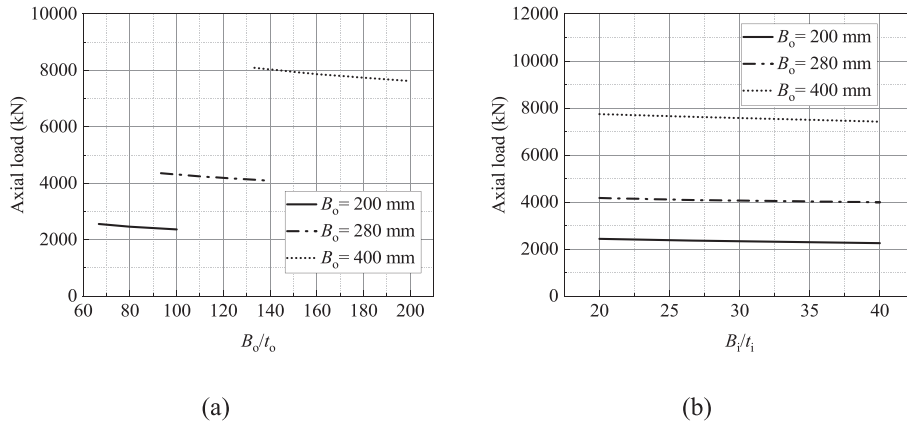
Fig. 26. Influence of (a) B_o/t_o and (b) B_i/t_i on the resistance of CFDSST columns.
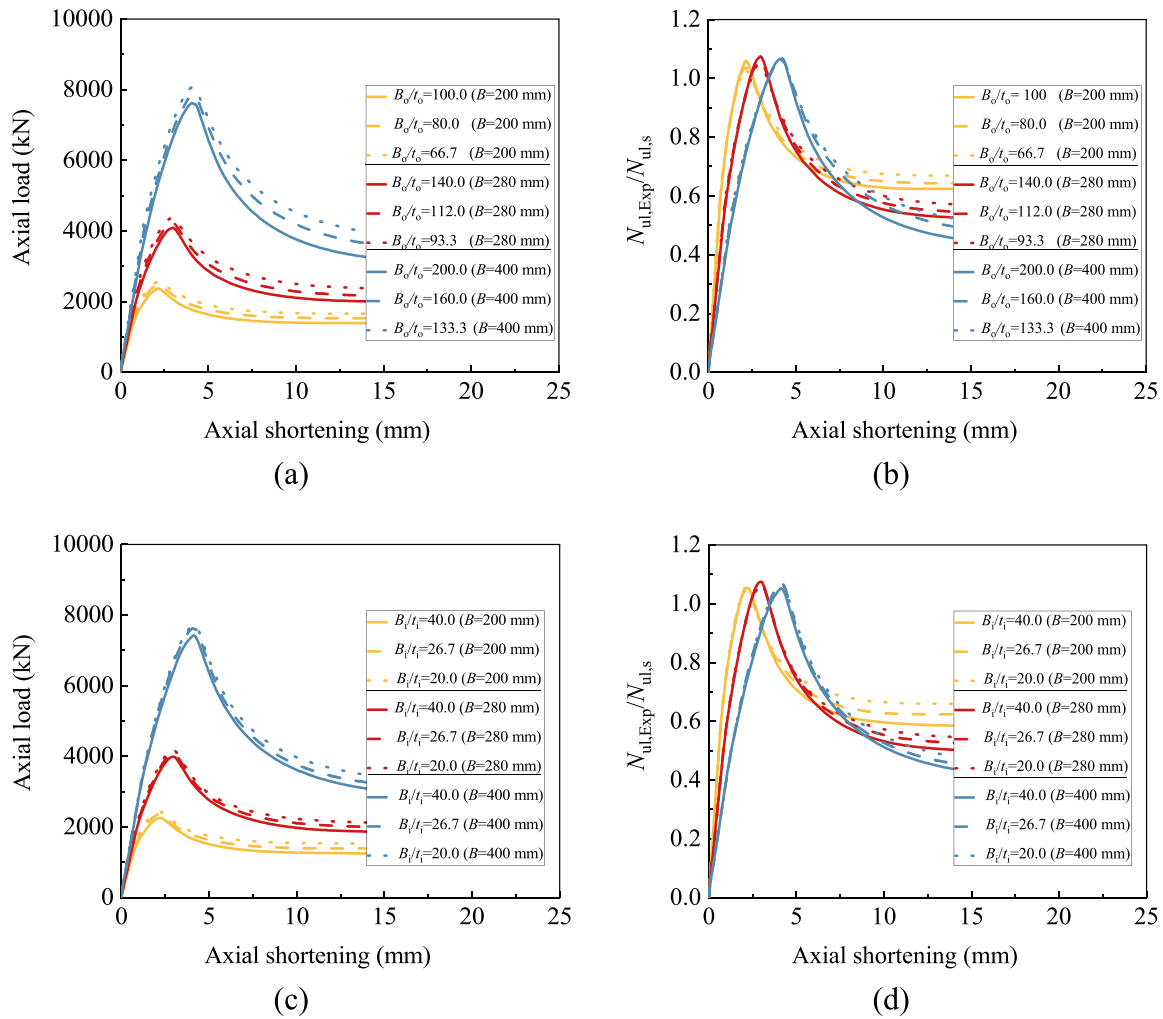
Fig. 27. Influence of (a and b) B_o/t_o and (c and d) B_i/t_i.

Fig. 28 presents the effect of χ on the resistance of CFDSST columns whilst Fig. 29 presents the influence of χ on the axial load *versus* displacement response. It is observed that the ultimate resistance increases marginally for CFDSSTs with higher B_i/B_o ratios. As before, the total cross-sectional area of concrete is the most influential parameter to the load-carrying capacity, and therefore it is not surprising that the B_i/B_o ratio has little influence, since the total concrete volume remains unchanged. With reference to Fig. 29, it is shown that the ductility and

post-failure load capacity generally increases for CFDSSTs with higher χ values. From Fig. 29(b), it is observed that the initial stiffness increases with a reduction in the cross-sectional width irrespective of the value of the hollow ratio χ. Moreover, increasing the hollow ratio χ of the columns results in relatively higher post-peak load behaviour, which may be attributed to the increase in the strength of the inner tubes.
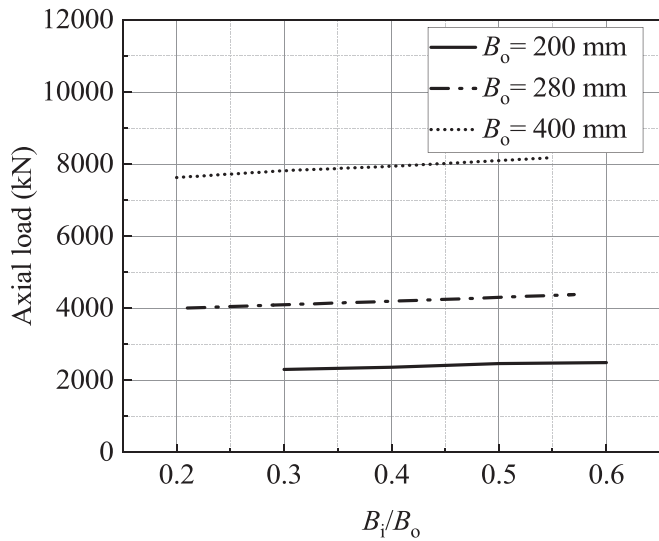
Fig. 28. Influence of hollow ratio on the resistance of CFDSST columns.

6. Design resistance

Currently, there are no design specifications available for CFDSST columns in the international design standards. The applicability of the design expressions given in Eurocode 4 [37], BS 5400 [38] and DBJ 1315–2010 [39], which were developed for CFST composite columns, was examined in the current study for CFDSST columns. The results are presented in Table 5, where $N_{ul,EC4}$, $N_{ul,BS5400}$ and $N_{ul,DBJ}$ represent the capacity values determined using Eurocode 4 [37], BS 5400 [38] and DBJ 1315–2010 [39], respectively. The following points are relevant to the calculations are results presented: (i) the effective area specified by Eurocode 3 [50] was employed to determine the cross-sectional area of the outer steel tube in these calculations, and (ii) the expressions given in Eurocode 4 [37] and BS 5400 [38] neglect the confinement effect of concrete for square cross-sections, while DBJ 1315–2010 [39] does take it into account.

6.1. Eurocode 4 [37]

The concrete compressive strength employed in the design expressions in Eurocode 4 [37] is equal to $0.85f_c$. The ultimate axial compressive resistance $N_{pl,Rd}$ is determined in accordance with Eq. (17),

which has been adapted for CFDSST columns and is given here as $N_{pl,EC4}$ in Eq. (18).

$$N_{pl,Rd} = A_a f_{yd} + 0.85 A_c f_{cd} + A_s f_{sd} \tag{17}$$

$$N_{ul,EC4} = A_{sy,eff} f_{yo} + A_{si} f_{yi} + A_{ss} f_{ys} + 0.85 A_{cs} f_{cs} + 0.85 A_{ci} f_{ci} \tag{18}$$

6.2. BS 5400 [38]

According to BS 5400 [38], the compressive resistance of CFDSST columns $N_{ul,BS5400}$ can be calculated in accordance with Eq. (19). It should be noted that the concrete cube strength (f_{cu}) is used in this equation and $f_{cu,s}$ and $f_{cu,i}$ represent the cube strength of the sandwiched concrete and the core concrete, respectively.

$$N_{ul,BS5400} = A_{sy,eff} f_{yo} + A_{ss} f_{ys} + A_{si} f_{yi} + 0.675 A_{cs} f_{cu,s} + 0.675 A_{ci} f_{cu,i} \tag{19}$$

6.3. DBJ 1315 [39]

The confinement effect of concrete is taken into account in this design method through a confinement factor ξ. The standard compressive strength of concrete (f_{ck}) is used and is taken as $0.67f_{cu}$. For CFDSST columns, the design resistance $N_{ul,DBJ}$ is given in Eq. (20) where $f_{ck,s}$ and $f_{ck,i}$ represent the standard compressive strength of the sandwiched concrete and core concrete, respectively.

$$N_{ul,DBJ} = (A_{sy,eff} + A_{cs})(1.18 + 0.85\xi_{so})f_{ck,s} + (A_{si} + A_{cc})(1.18 + 0.85\xi_{si})f_{ck,i} + A_{ss} f_{ys} \tag{20}$$

6.4. Results and discussion

The predictions of the ultimate resistance from each of the design codes is presented in Table 5. It is observed that Eurocode 4 and BS 5400 tend to provide rather conservative predictions, and underestimate the ultimate resistances of CFDSST columns by 17% on average. On the other hand, DBJ 1315 [39] provides quite accurate predictions with a mean $N_{ul,DBJ}/N_{ul,FE}$ ratio of 0.94 and a coefficient of variation (COV) of 0.036. The accuracy of this method compared with the others is attributed to the consideration given to the concrete confinement effect. In general, DBJ 1315 [39] provides the most suitable prediction for the ultimate resistance of CFDSST columns. In the above analysis, the buckling factor k_σ employed with Eq. (8) was taken as 4, assuming that $\psi = 1$. It was proposed by Uy and Bradford [59] that in the current scenario as the steel plates are in contact with a rigid medium, *i.e.* the concrete infill, a more suitable value for k_σ may be taken as 10.3. This
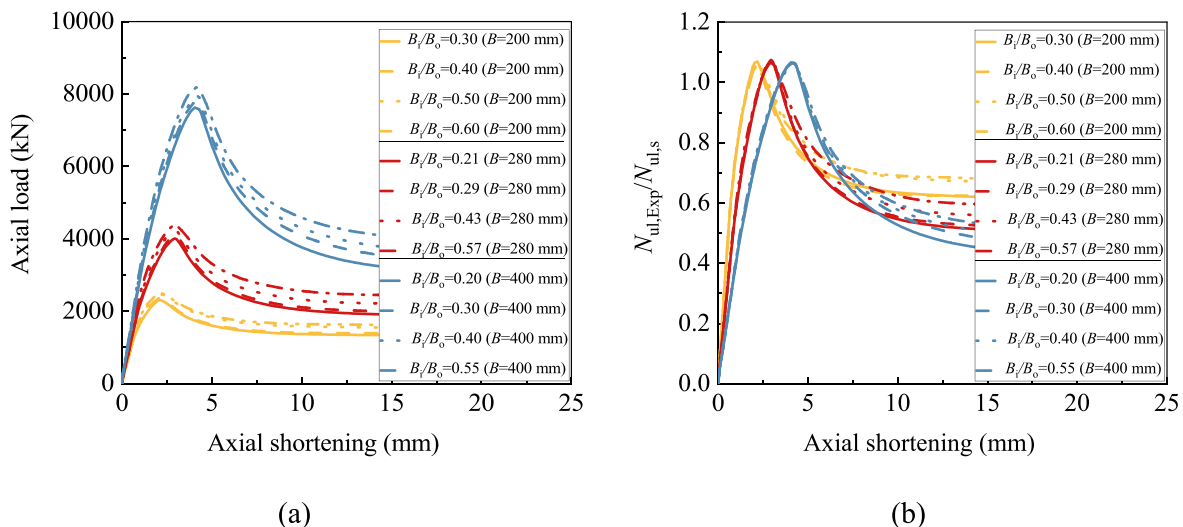

(a)

(b)

Fig. 29. Influence of hollow ratio on the (a) axial load and (b) normalised axial load, *versus* displacement responses of CFDSST columns.

Table 5

Design resistances from various international design codes.

Groups	Specimens	$N_{\mathrm{ul,FE}}$ (kN)	Eurocode 4 [37]		BS 5400 [38]		DBJ 1315 [39]	
			$\dfrac{N_{\mathrm{ul,EC4}}}{N_{\mathrm{ul,FE}}}$	$\dfrac{N_{\mathrm{ul,EC4}}}{N_{\mathrm{ul,FE}}}$	$\dfrac{N_{\mathrm{ul,BS5400}}}{N_{\mathrm{ul,FE}}}$	$\dfrac{N_{\mathrm{ul,BS5400}}}{N_{\mathrm{ul,FE}}}$	$\dfrac{N_{\mathrm{ul,DBJ}}}{N_{\mathrm{ul,FE}}}$	$\dfrac{N_{\mathrm{ul,DBJ}}}{N_{\mathrm{ul,FE}}}$
			$k_\sigma = 4.0$	$k_\sigma = 10.3$	$k_\sigma = 4.0$	$k_\sigma = 10.3$	$k_\sigma = 4.0$	$k_\sigma = 10.3$
	S1	2365	0.85	0.87	0.85	0.87	0.94	0.96
	S2	2609	0.83	0.88	0.83	0.88	0.89	0.94
	S3	2729	0.82	0.88	0.82	0.88	0.88	0.93
	S4	3005	0.79	0.87	0.79	0.86	0.83	0.89
	S5	3005	0.85	0.87	0.84	0.86	0.95	0.97
	S6	3587	0.86	0.87	0.86	0.87	0.98	1.00
	S7	4235	0.85	0.87	0.85	0.86	0.98	1.00
	S8	5106	0.87	0.88	0.86	0.87	1.01	1.02
	S9	2249	0.84	0.87	0.84	0.86	0.94	0.96
	S10	2425	0.85	0.88	0.85	0.87	0.94	0.96
	S11	2569	0.85	0.87	0.85	0.87	0.93	0.95
	S12	2465	0.85	0.88	0.85	0.87	0.95	0.97
G1	S13	2538	0.87	0.89	0.86	0.88	0.97	0.99
	S14	2601	0.88	0.90	0.88	0.90	1.00	1.02
	S15	2687	0.90	0.92	0.90	0.92	1.04	1.06
	S16	2371	0.84	0.86	0.84	0.86	0.93	0.95
	S17	2427	0.84	0.86	0.84	0.86	0.93	0.95
	S18	2456	0.84	0.87	0.84	0.86	0.93	0.95
	S19	2305	0.84	0.86	0.83	0.86	0.94	0.96
	S20	2464	0.85	0.87	0.84	0.87	0.92	0.94
	S21	2495	0.87	0.89	0.86	0.89	0.92	0.94
	S22	2460	0.88	0.88	0.87	0.88	0.95	0.96
	S23	2556	0.89	0.89	0.88	0.88	0.96	0.96
	S24	2254	0.85	0.87	0.85	0.87	0.93	0.95
	S25	2439	0.86	0.88	0.86	0.88	0.96	0.98
	S26	4091	0.82	0.85	0.82	0.85	0.93	0.96
	S27	4331	0.81	0.86	0.81	0.86	0.91	0.95
	S28	4510	0.80	0.85	0.80	0.85	0.89	0.93
	S29	4878	0.77	0.83	0.77	0.83	0.85	0.90
	S30	5451	0.83	0.86	0.83	0.85	0.95	0.98
	S31	6787	0.84	0.86	0.84	0.86	0.97	0.99
	S32	8197	0.84	0.86	0.83	0.85	0.97	0.99
	S33	10,180	0.85	0.86	0.84	0.86	0.99	1.01
	S34	3971	0.82	0.85	0.81	0.85	0.93	0.96
	S35	4153	0.82	0.86	0.82	0.85	0.93	0.96
	S36	4267	0.83	0.86	0.82	0.86	0.93	0.96
	S37	4173	0.83	0.86	0.82	0.86	0.94	0.97
G2	S38	4219	0.84	0.87	0.84	0.87	0.96	0.99
	S39	4250	0.86	0.89	0.85	0.88	0.98	1.01
	S40	4366	0.87	0.90	0.86	0.89	1.00	1.03
	S41	4045	0.82	0.86	0.82	0.85	0.93	0.96
	S42	4122	0.82	0.86	0.82	0.85	0.93	0.96
	S43	4181	0.83	0.86	0.82	0.85	0.93	0.96
	S44	4007	0.82	0.85	0.81	0.85	0.93	0.97
	S45	4223	0.83	0.86	0.83	0.86	0.92	0.95
	S46	4379	0.84	0.87	0.83	0.86	0.91	0.94
	S47	4235	0.83	0.87	0.83	0.86	0.93	0.97
	S48	4359	0.85	0.87	0.85	0.87	0.95	0.97
	S49	3991	0.82	0.85	0.81	0.85	0.92	0.95
	S50	4174	0.83	0.86	0.82	0.86	0.94	0.97
	S51	7625	0.82	0.84	0.81	0.83	0.93	0.95
	S52	8148	0.79	0.82	0.79	0.82	0.90	0.92
	S53	8407	0.78	0.81	0.78	0.81	0.88	0.91
	S54	8898	0.76	0.80	0.76	0.79	0.86	0.89
	S55	10,467	0.84	0.85	0.83	0.85	0.96	0.98
	S56	13,505	0.84	0.85	0.83	0.84	0.97	0.98
	S57	16,536	0.84	0.85	0.83	0.84	0.97	0.98
	S58	20,990	0.84	0.85	0.83	0.84	0.98	0.99
	S59	7501	0.81	0.84	0.81	0.83	0.93	0.96
G3	S60	7703	0.82	0.84	0.81	0.83	0.93	0.95
	S61	7822	0.82	0.84	0.81	0.84	0.93	0.95
	S62	7741	0.82	0.84	0.81	0.83	0.93	0.96
	S63	7789	0.82	0.84	0.82	0.84	0.94	0.97
	S64	7851	0.83	0.85	0.82	0.84	0.95	0.98
	S65	7924	0.84	0.86	0.83	0.85	0.97	0.99
	S66	7505	0.81	0.83	0.81	0.83	0.93	0.95
	S67	7488	0.82	0.85	0.82	0.84	0.94	0.96
	S68	7685	0.82	0.84	0.81	0.84	0.93	0.96
	S69	7817	0.82	0.84	0.81	0.83	0.93	0.95
	S70	7942	0.82	0.84	0.82	0.84	0.93	0.95

Table 5 (*continued*)

Groups	Specimens	$N_{\text{ul,FE}}$ (kN)	Eurocode 4 [37]		BS 5400 [38]		DBJ 1315 [39]	
			$\dfrac{N_{\text{ul,EC4}}}{N_{\text{ul,FE}}}$	$\dfrac{N_{\text{ul,EC4}}}{N_{\text{ul,FE}}}$	$\dfrac{N_{\text{ul,BS5400}}}{N_{\text{ul,FE}}}$	$\dfrac{N_{\text{ul,BS5400}}}{N_{\text{ul,FE}}}$	$\dfrac{N_{\text{ul,DBJ}}}{N_{\text{ul,FE}}}$	$\dfrac{N_{\text{ul,DBJ}}}{N_{\text{ul,FE}}}$
			$k_\sigma = 4.0$	$k_\sigma = 10.3$	$k_\sigma = 4.0$	$k_\sigma = 10.3$	$k_\sigma = 4.0$	$k_\sigma = 10.3$
	S71	8179	0.83	0.85	0.82	0.84	0.92	0.94
	S72	7866	0.82	0.85	0.81	0.84	0.93	0.96
	S73	8092	0.82	0.86	0.82	0.86	0.93	0.97
	S74	7426	0.82	0.85	0.82	0.84	0.94	0.96
	S75	7745	0.82	0.84	0.81	0.83	0.93	0.96
Mean			**0.83**	**0.86**	**0.83**	**0.86**	**0.94**	**0.96**
COV			**0.029**	**0.023**	**0.029**	**0.024**	**0.036**	**0.030**
Min			**0.76**	**0.80**	**0.76**	**0.79**	**0.83**	**0.89**
Max			**0.90**	**0.92**	**0.90**	**0.92**	**1.04**	**1.06**

Table 6

Comparison of experimental and numerical resistances of test specimens with those obtained from international specifications [37–39] with $k_\sigma = 10.3$.

Groups	specimens	$N_{\text{ul,Exp}}$ (kN)	$N_{\text{ul,FE}}$ (kN)	Eurocode 4 [37]			BS 5400 [38]			DBJ 1315 [39]		
				$N_{\text{ul,EC4}}$ (kN)	$\dfrac{N_{\text{ul,EC4}}}{N_{\text{ul,Exp}}}$	$\dfrac{N_{\text{ul,EC4}}}{N_{\text{ul,FE}}}$	$N_{\text{ul,BS5400}}$ (kN)	$\dfrac{N_{\text{ul,BS5400}}}{N_{\text{ul,Exp}}}$	$\dfrac{N_{\text{ul,BS5400}}}{N_{\text{ul,FE}}}$	$N_{\text{ul,DBJ}}$ (kN)	$\dfrac{N_{\text{ul,DBJ}}}{N_{\text{ul,Exp}}}$	$\dfrac{N_{\text{ul,DBJ}}}{N_{\text{ul,FE}}}$
G3	SS-160-1	2090	1970	1775	0.85	0.90	1769	0.85	0.90	1911	0.91	0.97
	SS-160-2	2066	2070	1854	0.90	0.90	1847	0.89	0.89	2012	0.97	0.97
	SS-160-3	2770	2435	2160	0.78	0.89	2151	0.78	0.88	2407	0.87	0.99
G4	SS-160-4	2147	2111	1935	0.90	0.92	1929	0.90	0.91	2088	0.97	0.99
	SS-160-5	2237	2313	2174	0.97	0.94	2168	0.97	0.94	2278	1.02	0.98
	SS-160-6	1878	1940	1767	0.94	0.91	1761	0.94	0.91	1977	1.05	1.02
	SS-160-7	2025	2184	2007	0.99	0.92	2001	0.99	0.92	2186	1.08	1.00
G5	SS-180-1	2389	2302	2053	0.86	0.89	2045	0.86	0.89	2236	0.94	0.97
	SS-180-2	2441	2408	2155	0.88	0.89	2147	0.88	0.89	2365	0.97	0.98
	SS-180-3	3167	2890	2551	0.81	0.88	2540	0.80	0.88	2866	0.91	0.99
G5	SS-180-4	2336	2451	2213	0.95	0.90	2205	0.94	0.90	2414	1.03	0.98
	SS-180-5	2447	2718	2477	1.01	0.91	2469	1.01	0.91	2631	1.08	0.97
	SS-180-6	2118	2278	2046	0.97	0.90	2038	0.96	0.89	2298	1.09	1.01
	SS-180-7	2404	2534	2309	0.96	0.91	2302	0.96	0.91	2534	1.05	1.00
Mean					**0.91**	**0.90**		**0.91**	**0.90**		**1.00**	**0.99**
COV					**0.077**	**0.017**		**0.077**	**0.017**		**0.072**	**0.015**
Min					**0.78**	**0.88**		**0.78**	**0.88**		**0.87**	**0.97**
Max					**1.01**	**0.94**		**1.01**	**0.94**		**1.09**	**1.02**

was employed elsewhere also [60], and more accurate and appropriate results were obtained. This value has been applied to the current analysis and the results are presented in Table 6. It is shown that employing $k_\sigma = 10.3$ provides better resistance values and DBJ 1315 [39] still provides the most accurate predictions.

7. Conclusions

This paper presents a detailed description of a series of tests on cold-formed concrete-filled dual steel stiffened tubular (CFDSST) short columns under axial compressive load. These are very efficient members, which offer several advantages over existing typologies of composite column in terms of load-bearing capacity and resistance to local buckling. The tests results are analysed, and it is shown that the strength of the concrete is the most important factor to the overall capacity, and this is fully exploitable through the presence of the stiffened outer tube which provides confinement. The stiffeners also delay or prevent outward buckling of the steel section under compressive load. In addition to the experimental campaign, a detailed numerical investigation was also conducted and discussed here, and both the experimental and numerical findings were employed to examine the validity of existing design expressions. The following important conclusions are observed from the results presented:

(1) The experimental test results indicate that CFDSST columns exhibit higher strength and superior ductility than concrete-filled stiffened steel tubular (CFSST) columns due to the presence of the inner square CFST component. All of the test specimens failed by local outward buckling of the outer steel tube, and no steel fracture was found in the corners and welds of the test specimens.

(2) The parametric study showed that increasing the sandwiched concrete strength (f_{cs}) effectively increase the axial resistance of CFDSST columns. Additionally, it was found that decreasing the B_o/t_o ratio and increasing the B_i/B_o ratio and yield strength of the outer tube (f_{yo}) can increase the ductility and post-failure load capacity of the CFDSST columns.

(3) Based on the resistance comparisons of the experimental and numerical resistance values with the predictions from international design codes, it was shown that Eurocode 4 [37] and BS 5400 [38] provide overly conservative predictions. On the other hand, DBJ 1315–2010 [39] provides the most accurate ultimate resistance values for the CFDSST short columns, using a buckling factor of $k_\sigma = 10.3$ which is appropriate for steel plates in contact with a rigid medium. The better performance of this code, compared to the approaches in Eurocode 4 and BS 5400 is attributed to the inclusion of a parameter to account for confinement of the concrete, which is provided by the steel tubes.

CRediT authorship contribution statement

Jun-Hua Zhang: Data curation, Formal analysis, Investigation, Methodology, Writing – original draft. **Yong-Bo Shao:** Conceptualization, Data curation, Formal analysis, Methodology, Visualization, Writing – original draft. **M.F. Hassanein:** Conceptualization,

Investigation, Methodology, Project administration, Resources, Supervision, Visualization, Writing – review & editing. **K.A. Cashell:** Investigation, Methodology, Supervision, Validation, Writing – review & editing. **Marijana Hadzima-Nyarko:** Methodology, Supervision, Validation.

Declaration of Competing Interest

The authors declare that they have no known competing financial interests or personal relationships that could have appeared to influence the work reported in this paper.

Data availability

Data will be made available on request.

Acknowledgement

References

[1] J. Zeghiche, K. Chaoui, An experimental behaviour of concrete-filled steel tubular columns, J. Constr. Steel Res. 61 (1) (2005) 53–66.

[2] C. Huang, X.L. Han, J. Ji, et al., Behavior of concrete-filled steel tubular planar intersecting connections under axial compression. Part 1: experimental study, Eng. Struct. 32 (1) (2010) 60–68.

[3] J.F. Dong, Q.Y. Wang, Z.W. Guan, Structural behaviour of recycled aggregate concrete filled steel tube columns strengthened by CFRP, Eng. Struct. 48 (2013) 532–542.

[4] L.H. Guo, S.M. Zhang, W.J. Kim, et al., Behavior of square hollow steel tubes and steel tubes filled with concrete, Thin-Walled Struct. 45 (12) (2007) 961–973.

[5] M.H. Lai, J.C.M. Ho, A theoretical axial stress-strain model for circular concrete-filled-steel-tube columns, Eng. Struct. 125 (2016) 124–143.

[6] B. Uy, Local and post-local buckling of concrete filled steel welded box columns, J. Constr. Steel Res. 47 (1–2) (1998) 47–72.

[7] M.A. Dabaon, M.H. EI-Boghdadi, M.F. Hassanein, Experimental investigation on concrete-filled stainless steel stiffened tubular stub columns, Eng. Struct. 31 (2) (2009) 300–307.

[8] X. Chang, Y.Y. Wei, Y.C. Yun, Analysis of steel-reinforced concrete-filled-steel tubular (SRCFST) columns under cyclic loading, Constr. Build. Mater. 28 (1) (2012) 88–95.

[9] J.M. Cai, J.L. Pan, Y.F. Wu, Mechanical behaviour of steel-reinforced concrete-filled-steel tubular (SRCFST) columns under uniaxial compressive loading, Thin-Walled Struct. 97 (2015) 1–10.

[10] J.P. Liu, P. Gao, X.C. Lin, et al., Experimental assessment on the size effects of circular concrete-filled steel tubular columns under axial compression, Eng. Struct. 275 (2023), 115247.

[11] P. Gao, X.H. Zhou, J.P. Liu, et al., Experimental assessment on the size effects of square concrete-filled steel tubular columns under axial compression, Eng. Struct. 281 (2023), 115706.

[12] M.H. Lai, J.C.M. Ho, Confinement effect of ring-confined concrete-filled-steel-tube columns under uni-axial load, Eng. Struct. 67 (2014) 123–141.

[13] M.X. Xiong, D.X. Xiong, J.Y. Richard Liew, Axial performance of short concrete filled steel tubes with high-and ultra-high-strength materials, Eng. Struct. 136 (2017) 494–510.

[14] T.T. Nguyen, H.T. Thai, T. Ngo, B. Uy, D.X. Li, Behaviour and design of high strength CFST columns with slender sections, J. Constr. Steel Res. 130 (2021), 107282.

[15] Z. Tao, L.H. Han, D.Y. Wang, Experimental behaviour of concrete-filled stiffened thin-walled steel tubular columns, Thin-Walled Struct. 45 (5) (2007) 517–527.

[16] Z. Zhou, M.D. Denavit, X.H. Zhou, New cross-sectional slenderness limits for stiffened rectangular concrete-filled steel tubes, Eng. Struct. 280 (2023) 0141–0296.

[17] Y. Xu, Y.B. Shao, M.F. Hassanein, N. Silvestre, Innovative compressive design resistance and behaviour of concrete-filled short columns with Stiffened Square steel sections, J. Constr. Steel Res. 198 (2022), 107510.

[18] M.A. Dabaon, S. El-Khoriby, M.H. EI-Boghdadi, M.F. Hassanein, Confinement Effect of Stiffened and Unstiffened Concrete-Filled Stainless Steel Tubular Stub Columns, J. Constr. Steel Res. 65 (8–9) (2009) 1846–1854.

[19] C.Y. Wan, X.X. Zha, Nonlinear analysis and design of concrete-filled dual steel tubular columns under axial loading, Steel Compos. Struct. 20 (3) (2016) 571–597.

[20] T. Ekmekyapar, B.J.M. Al-Eliwi, Concrete filled double circular tube (CFDCST) stub columns, Eng. Struct. 135 (0) (2017) 68–80.

[21] X.D. Fang, S.J. Lin, Axial compressive test of columns with multi barrel tube-confined high performance concrete, J. Build. Struct. 35 (4) (2014) 236–245.

[22] X. Chang, Z.L. Ru, W. Zhou, et al., Study on concrete-filled stainless steel-carbon steel tubular (CFSCT) stub columns under compression, Thin-Walled Struct. 63 (2013) 125–133.

[23] M.F. Hassanein, O.F. Kharoob, Q.Q. Liang, Behaviour of circular concrete-filled lean duplex stainless steel-carbon steel tubular short columns, Eng. Struct. 56 (2013) 83–94.

[24] J.R. Qian, Y. Zhang, X.D. Ji, et al., Test and analysis of axial compressive behaviour of short composite-sectioned high strength concrete filled steel tubular columns, J. Build. Struct. 12 (2011) 162–169 (in Chinese).

[25] M. Ahamed, Q.Q. Liang, V.I. Patel, et al., Nonlinear analysis of rectangular concrete-filled double steel tubular short columns incorporation local buckling, Eng. Struct. 175 (2018) 13–26.

[26] J.C. Ci, S.C. Chen, H. Jia, et al., Axial compression performance analysis and bearing capacity calculation on square concrete-filled double-tube short columns, Mar. Struct. 72 (2020), 102775.

[27] F.X. Ding, W.J. Wang, X.M. Liu, et al., Mechanical behaviour of outer square inner circular concrete-filled dual steel tubular stub columns, Steel Compos. Struct. 38 (3) (2021) 305–317.

[28] Z. Tao, L.H. Han, Z.B. Wang, Experimental behaviour of stiffened concrete-filled thin-walled hollow steel structural (HSS) stub columns, J. Constr. Steel Res. 61 (7) (2005) 962–983.

[29] Z. Tao, L.H. Han, D.Y. Wang, Experimental behaviour of concrete-filled stiffened thin-walled steel tubular columns, Thin-Walled Struct. 45 (5) (2007) 517–527.

[30] B. Wang, J.H. Liang, Z. Lu, Experimantal investigation on seismic behaviour of square CFT columns with different shear stud layout, J. Constr. Steel Res. 153 (2019) 130–138.

[31] C. Hou, L.-H. Han, X.-L. Zhao, Concrete-filled circular steel tubes subjected to local bearing force: experiments, J. Constr. Steel Res. 83 (2013) 90–104.

[32] Z.B. Wang, Z. Tao, Q. Yu, Axial compressive behaviour of concrete-filled double-tube stub columns with stiffeners, Thin-Walled Struct. 120 (2017) 91–104.

[33] Z.B. Wang, F.B. Wei, S.Y. Chi, et al., Study on behaviour of composite concrete-filled square thin-walled steel tubular columns under eccentrical compression, J. Hunan Univ. (Nat. Sci.) 45 (9) (2018) 20–29 (in Chinese).

[34] Z.B. Wang, W.A. Zhang, S.Y. Chi, et al., Flexural behaviour of composite concrete-filled square thin-walled steel tubular specimens, J. Build. Struct. 38 (7) (2017) 78–84 (in Chinese).

[35] Z.B. Wang, H.J. Wu, J.P. Zhuang, et al., Seismic behaviour of concrete-filled thin-walled double-tubular columns with longitudinal stiffeners, J. Build. Struct. 40 (11) (2020) 41–50 (in Chinese).

[36] J.H. Zhang, Y.B. Shao, M.F. Hassanein, et al., Axial compressive performance of ultra-high strength concrete-filled dual steel tubular short columns with outer stiffened tubes and inner circular tubes, J. Constr. Steel Res. 203 (2023) 0143–974X.

[37] Eurocode 4, Design of composite steel and concrete structures, Part1.1, General rules and rules for building, British Standards Institution, London, 2023 (BS EN 1994-1-1: 2004).

[38] BS5400, Steel, Concrete and Composite Bridges, Part 5, Code of Practice for Design of Composite Bridges, British Standards Institution, London, 1979.

[39] DBJ/T13-51-2010, Technical specification for concrete-filled steel tubular structures, The Construction Department of Fujian Province, Fuzhou (China), 2003 [in Chinese].

[40] Z. Tao, L.H. Han, Z.B. Wang, Experimental behaviour of stiffened concrete-filled thin-walled hollow steel structural (HSS) stub columns, J. Constr. Steel Res. 61 (7) (2005) 962–983.

[41] Australian Standard, Methods for Tensile Testing of Metals, AS 1391, Standards Association of Australia, Sydney (Australia), 1991.

[42] L.-H. Han, G.-H. Yao, Influence of concrete compaction on the strength of concrete-filled steel RHS columns, J. Constr. Steel Res. 59 (2003) 751–767.

[43] J.P. Liu, X.H. Zhou, D. Gan, Effect of friction on axially loaded stub circular tubed columns, Adv. Struct. Eng. 19 (3) (2016) 546–559.

[44] R. Rohola, C. Hélder, S. Rui, L. Luís, S. Aldina, Buckling resistance of concrete-filled cold-formed steel (CF-CFS) built-up short columns under compression, Thin-Walled Struct. 170 (2022), 0263-8231.

[45] Z. Tao, B. Uy, L.H. Han, et al., Analysis and design of concrete-filled stiffened thin-walled steel tubular columns under axial compression, Thin-Walled Struct. 47 (12) (2009) 1544–1556.

[46] Z. Tao, Z.B. Wang, Q. Yu, Finite element modelling of concrete-filled steel stub columns under axial compression, J. Constr. Steel Res. 89 (2013) 121–131.

[47] R. Zhang, S. Chen, P. Gu, Y. Huang, Structural behaviour of UHPC filled steel tubular columns under eccentric loading, Thin-Walled Struct. 156 (2020) 106959.

[48] G.C. Li, B.W. Chen, Z.J. Yang, Y.P. Liu, Y.H. Feng, Experimental and numerical behaviour of eccentrically loaded square concrete-filled steel tubular long columns made of high-strength steel and concrete, Thin-Walled Struct. 159 (2021) 107289.

[49] J.B. Yan, A. Chen, J.S. Zhu, Behaviours of square UHPFRC-filled steel tubular stub columns under eccentric compression, Thin-Walled Struct. 159 (2021) 107222.

[50] Eurocode 3, Design of Steel Structures, Part4.4, Plate Elements without Longitudinal Stiffeners, British Standards Institution, London, 1997 (BS EN 1993-1-5: 1997).

[51] ABAQUS, ABAQUS Standard User's Manual, Version 2020, Dassault Systèmes Corp, Providence (RI, USA), 2020.

[52] M.F. Hassanein, M. Elchalakani, A. Karrech, et al., Behaviour of concrete-filled double-skin short columns under compression through finite element modelling: SHS outer and SHS inner tubes, Structures 14 (1) (2018) 358–375.

[53] L.H. Han, G.H. Yao, Z. Tao, Performance of concrete-filled thin-walled steel tubes under pure torsion, Thin-Walled Struct. 45 (1) (2007) 24–36.

[54] B. Uy, Concrete-filled fabricated steel box columns for multistorey buildings: behaviour and design, Prog. Struct. Eng. Mater. 1 (2) (1998) 150–158.

[55] L.H. Han, Concrete Filled Steel Tubular Columns-Theory and Practice, 2nd ed, Science Press, Beijing, 2007 (in Chinese).

[56] L.-H. Han, C. Hou, Y.-X. Hua, Concrete-filled steel tubes subjected to axial compression: life-cycle based performance, J. Constr. Steel Res. 169 (2020) 106063.

[57] J.Y.R. Liew, D.X. Xiong, Ultra-high strength concrete filled composite columns for multi-storey building construction, Adv. Struct. Eng. 15 (9) (2012) 1487–1503.

[58] Eurocode 2, Design of concrete structures. Part 1–1. General rules and rules for, buildings, 2004.

[59] B. Uy, M.A. Bradford, Elastic local buckling of steel plates in composite steel-concrete members, Eng. Struct. 18 (3) (1996) 193–200.

[60] A.R. Elsisy, Y.-B. Shao, M. Zhou, M.F. Hassanein, A study on the compressive strengths of stiffened and unstiffened concrete-filled austenitic stainless steel tubular short columns, Ocean Eng. 248 (2022) 110793.